Self-metalation of 2H-Tetraphenylporphyrin on Cu(111): an X-ray spectroscopy study

K. Diller,[1, a)] F. Klappenberger,[1] M. Marschall,[1] K. Hermann,[2] A. Nefedov,[3] Ch. Wöll,[3] and J. V. Barth[1]

[1)] *Physik Department E20, Technische Universität München, James-Franck-Straße 1, D-85748 Garching, Germany*

[2)] *Fritz-Haber-Institut der Max-Planck-Gesellschaft, Faradayweg 4-6, D-14195 Berlin, Germany*

[3)] *Institut für Funktionelle Grenzflächen (IFG), Karlsruher Institut für Technologie (KIT), Hermann-von-Helmholtz-Platz 1, D-76344 Eggenstein-Leopoldshafen, Germany*

The bonding and the temperature-driven metalation of 2H-Tetraphenylporphyrin (2H-TPP) on the Cu(111) surface under ultrahigh vacuum (UHV) conditions were investigated by a combination of X-ray photoelectron spectroscopy (XPS) and near-edge X-ray absorption fine structure (NEXAFS) spectroscopy with density functional theory (DFT) calculations. Thin films were prepared by organic molecular beam epitaxy and subsequent annealing. Our systematic study provides an understanding of the changes of the spectroscopic signature during adsorption and metalation. Specifically, we achieved a detailed peak assignment of the 2H-TPP multilayer data of the C1s and the N1s region. After annealing to 420 K both XPS and NEXAFS show the signatures of a metalloporphyrin, which indicates self-metalation at the porphyrin-substrate interface, resulting in Cu-TPP. Furthermore, for 2H-TPP monolayer samples we show how the strong influence of the copper surface is reflected in the spectroscopic signatures. Adsorption results in a strongly deformed macrocycle and a quenching of the first NEXAFS resonance in the nitrogen edge suggesting electron transfer into the LUMO. For Cu-TPP the spectroscopic data indicate a reduced interaction of first-layer molecules with the substrate as demonstrated by the relaxed macrocycle geometry.

I. INTRODUCTION

The interaction of complex molecular species with solid substrates is a key issue in the development of functional interfaces[1] and plays an essential role in the deliberate construction of nanoscale architectures on surfaces.[2] Molecule-surface interactions influence the conformation of the adsorbed molecules,[3] their magnetic properties[4] as well as their electronic structure, for example by charge transfer processes.[5,6] A class of molecules which promises numerous applications is given by the porphyrins as they exhibit a large variety of functional properties which can be tuned by changing the meso-substituents or the metal center of the molecule. Metalloporphyrin compounds notably combine an active site (the central metal atom) embedded in a robust tetrapyrrolic macrocycle suggesting nanoscale applications[7,8] like chemosensors[9,10] or the usage as active catalytic sites[11–13]. Their photophysical properties make them promising candidates for the development of optical devices like organic solar cells[14,15] or organic light emitting diodes[16]. Moreover, porphyrins adsorbed at metal surfaces offer a rich playground for the exploration of model interfacial coordination systems.[17–21] To this end it is of crucial importance to cope with their electronic properties[22–24] and inherent conformational flexibility, which can interfere in supramolecular organization[25,26] and allow for unconvential ligation modes of adducts[27,28].

To investigate metalloporphyrin-substrate interactions premanufactured molecules can be used.[29] Alternatively it is possible to evaporate free-base porphyrins and metalate them directly on the surface which allows to prepare films of metalloporphyrins whose instability or reactivity prevent a direct evaporation. The metalation so far mainly has been realized by vapor deposition of free-base porphyrins and metal atoms including Fe[30–32], Zn[33], Co[34], Ni[35] and Ce[36,37]. A different approach is the self-metalation at the porphyrin-substrate

interface, i.e., the metalation of the free-base porphyrins with surface atoms without utilizing additionally evaporated metal atoms. So far, this has been reported only for the system H2PPIX on Cu(110) and Cu(100).[38]

In this work we demonstrate that self-metalation of mono- and even multilayers of free-base porphyrins is possible on the dense-packed Cu(111) surface. We use a multitechnique approach combining X-ray photoelectron spectroscopy (XPS) and near-edge X-ray absorption fine structure (NEXAFS) spectroscopy with density functional theory (DFT) calculations on isolated free-base meso tetraphenylporphyrin (2H-TPP, Fig. 1a) and copper tetraphenylporphyrin (Cu-TPP, Fig. 1b) molecules. We deposited 2H-TPP molecules on the Cu(111) surface and followed the changes of the spectroscopic signatures during the temperature driven self-metalation.

While XPS[32,34,35] and NEXAFS[32,39–42] experimental data are sufficient to obtain information about (metallo)porphyrins, the combination with DFT calculations provide additional insight and a comprehensive basis for the interpretation of the spectral features.[43–45] Here, the combined analysis and the comparison of experimental with simulated spectra allows us to disentangle the complex NEXAFS features and thus to understand the structural and electronic properties of metalated and nonmetalated species in mono- and multilayer samples.

II. EXPERIMENTAL DETAILS

The data were taken at the HE-SGM beamline at BESSY II in Berlin. All experiments were performed in an ultrahigh vacuum (UHV) system with a base pressure in the low 10^{-10} mbar regime. The Cu(111) single crystal surface (Surface Preparation Laboratory, polished to $< 0.5°$) was prepared by repeated cycles of Ar^+ sputtering at 1 keV and sub-

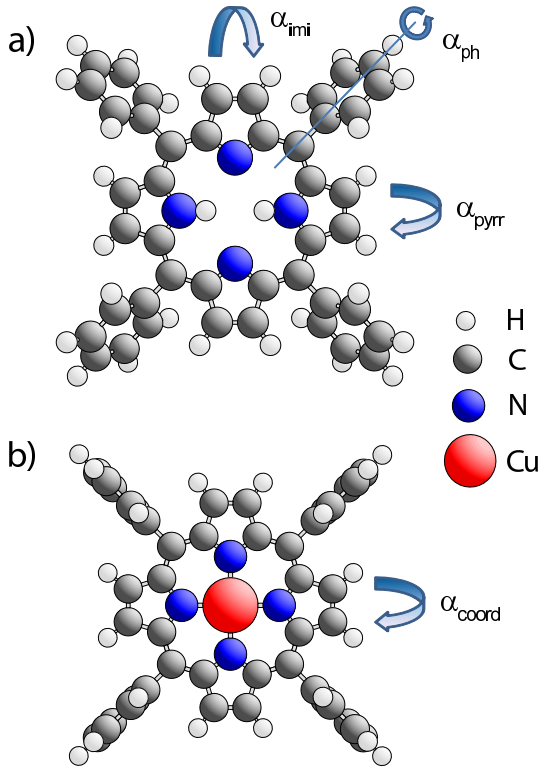

FIG. 1. Models of a) free-base tetraphenylporphyrin (2H-TPP) and b) copper tetraphenylporphyrin (Cu-TPP) displayed with conformations obtained by geometry optimization of isolated molecules. The angles α_{imi}, α_{pyrr} and α_{coord} describe the inclination of the respective pyrrole rings out of the macrocycle plane, while α_{ph} refers to the rotation of a phenyl ring around the C-C bond that connects it to the macrocycle. The model in b) is characterized by $\alpha_{coord} = 0$ and $\alpha_{ph} = 90°$.

sequent annealing at 720 K. The 2H-TPP molecules (Sigma-Aldrich) were deposited by organic molecular beam epitaxy from a boron nitride crucible held at 600 K onto the substrate which was kept at 220 K. Prior to the experiments the porphyrins were degassed in vacuo by heating them up to 520 K for several hours. The layer-thicknesses were calibrated against the XPS signals of a monolayer of 2H-TPP that was obtained by annealing a multilayer to 550 K. We thus use the term monolayer (ML) for the maximum coverage of molecules directly adsorbed on the surface. Average evaporation rates for a sublimation temperature of 600 K were 0.07 ML/min. The sample was kept at 200 K during the measurements.

For the XPS measurements a photon energy of 550 eV was used for the N1s and 435 eV for the C1s measurements. The monochromator grating with 1500 l/mm, the slit widths of 200 µm and the pass energy of the hemispherical analyzer of 50 eV resulted in a total resolution of 0.8 eV for the N1s and 0.6 eV for the C1s region. If not otherwise noted analyzer and sample were adjusted for normal electron emission. All binding energies were referenced against the $Cu3p_{3/2}$ line (at 75.1 eV) of the substrate as the photon range of the beamline did not allow to investigate the sharp Cu2p lines. After subtracting a linear background from the raw data, the data were fitted using Voigt curves.

NEXAFS data were taken in the partial electron yield (PEY) mode with a retarding voltage of -250 V for the N K-edge and -150 V for the C K-edge. With the same grating and slits settings, energy resolution was approximately the same as for XPS. The incidence angle θ between the surface normal and the $\vec{E}$-vector of the linear polarized light was varied by rotating the sample with respect to the incoming beam. For the given polarization (90% if not otherwise noted) the magic angle at which every resonance appears in the spectrum independent of the orientation of the corresponding orbital amounts to 53°. For each of the three different angles (cf. Fig. 4 and Fig. 5) several spectra were recorded and

averaged to improve the signal to noise ratio and to verify that no beam damage occurred. Simultaneously to the PEY spectra the photocurrent signal of a gold grid traversed by the X-ray beam was recorded. After referencing the energy scale against characteristic peaks (399 eV for nitrogen, 285 eV for carbon) of the Au grid spectrum, the signal of the bare crystal was subtracted from the sample spectrum, followed by a correction for the photon flux and a normalization of the edge jump to one (according to ref. 46).

III. COMPUTATIONAL DETAILS

The calculations for the isolated molecules 2H-TPP, Cu-TPP and 2H-TPP with removed inner hydrogens (in the following denoted as TPP) were performed with the density functional theory (DFT) program package StoBe[47] using a revised Perdew, Burke and Ernzerhof (RPBE) exchange-correlation functional.[48,49] The Kohn–Sham orbitals were described by linear combinations of atomic orbitals (LCAOs).

The geometries of the molecules were optimized in a first step using all-electron triple-zeta plus valence polarization (TZVP) type basis sets[50,51] to describe the nitrogen, carbon,[50] and hydrogen[51]. The starting geometry was that of a porphyrin with a saddle-shaped conformation which was reported for adsorbed Co-TPP on Ag(111)[29] and TPyP on Cu(111)[52]. The vibrational analysis of the optimized geometries shows no negative frequencies which excludes the possibility that the optimization routine merely converged to a saddle point. Bond lengths and angles agree well with the solid state structures of 2H-TPP and Cu-TPP determined by X-ray diffraction (cf. refs. 53 and 54).

The basis sets used in the electronic structure calculations for the ground state and the core excitations were chosen dependent on the excitation center. For excitations at a given nitrogen or carbon center the basis set at that center is of all-electron individual gauge

for localized orbitals (IGLO)-III quality[55] yielding an improved representation of relaxation effects in the inner atomic shells. The other atoms of the same element type in the molecule are described by effective core potentials (ECP) for the 1s core and appropriate valence basis sets.[56] The use of ECPs simplifies the identification of the core hole orbital while it has only negligible effects on the computed excitation spectrum.[57] In addition, large diffuse even-tempered [19s19p19d] basis sets[58] are included at the excitation center for a more accurate calculation of transition moments and excitation energies involving Rydberg and continuum final states (double basis set technique[58]).

Ionization energies were obtained by subtracting the calculated total energies of the core hole state from that of the ground state:

$$E_{ion} = E_{tot}(n_{1s} = 1) - E_{tot}(n_{1s} = 0) \tag{1}$$

The calculations of the absorption spectra used the transition potential (TP) approximation[59,60] where the occupation of the 1s core orbital at the excitation center is set to $n = 0.5$. This approach allows the calculation of all final states in one single SCF calculation (and accounts for relaxation up to second order[60]) enabling the calculation of absorption spectra of big molecules like porphyrins within a reasonable computational time. Further details of the method are described in ref. 60. The discrete excitation energies and corresponding dipole transition matrix elements obtained in the calculations are convoluted with Gaussians of varying width to obtain continuous spectra for comparison with experiment. The broadening width was fixed at 0.5 eV for excitations below the ionization threshold while it was assumed to increase linearly up to 4.5 eV between the threshold and 10 eV above after which it was kept constant at 4.5 eV. This procedure accounts for the increasing width of σ^* resonances due to their reduced lifetime.[46]

The missing core hole relaxation of the excited final state due to its transition potential

(TP) treatment can be taken into account in an approximate way by shifting all exciatation energies by the difference between the ionization potential obtained in the TP calculation and that for the fully relaxed core hole configuration evaluated self-consistently (eq. 1). This yields shifts to lower excitation energies by 1.4 eV for carbon and 1.6 eV for nitrogen 1s excitations. Further, relativistic corrections are accounted for by an additional global spectral shift by 0.1 eV and 0.3 eV for carbon and nitrogen, respectively.[61] The resulting theoretical carbon spectra on an absolute energy scale differ overall from experimental data by about 0.4 eV (shifts to higher energy) which may be due to both numerical basis set effects and/or experimental calibration. For easier comparison this 0.4 eV shift is included in Fig. 6.

IV. RESULTS AND DISCUSSION

A. Self-Metalation

In previous studies porphyrins have been metalated by coevaporating molecules and metal atoms on the substrate sometimes followed by an annealing step.[30–34] In this work the self-metalation, i.e., the metalation of adsorbed free-base porphyrins by substrate atoms, is studied. 2H-TPP layers of different thicknesses were prepared on the Cu(111) surface. Taking into account the different scattering cross sections, the XPS peak area ratio for the N1s and C1s signals was in agreement with the expected value of 11 (44 carbon, 4 nitrogen atoms) for all samples. No signals other than of Cu, N and C were detected. The ratio and the absence of contaminations indicate the controlled evaporation of intact molecules.

After the deposition of a 2H-TPP multilayer the N1s XPS spectrum shows two principal peaks (Fig. 2a) as expected from the nonequivalence of the nitrogen atoms in the 2H-TPP

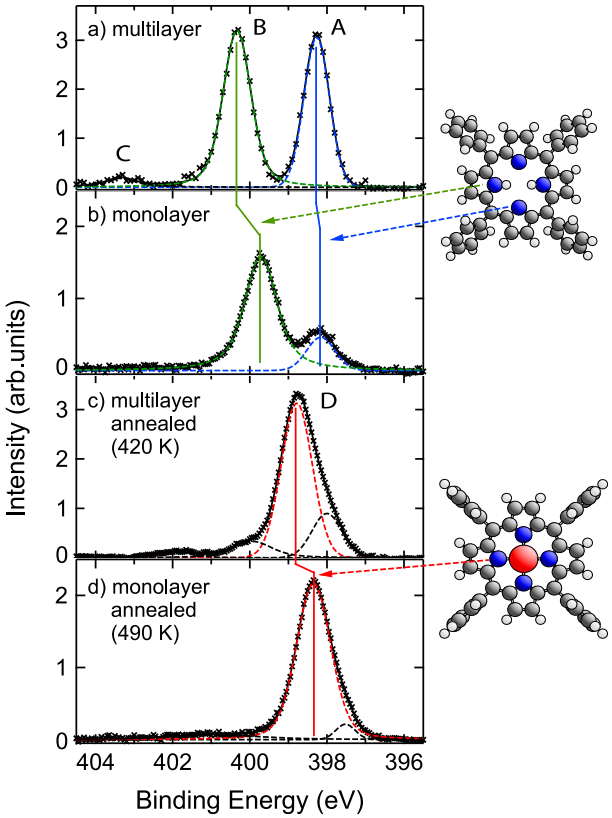

FIG. 2. The N1s XPS spectra of (a) a 2H-TPP multilayer and (b) a 2H-TPP monolayer adsorbed on Cu(111) show two peaks that are assigned to iminic (A, blue) and pyrrolic (B, green) nitrogen species. After annealing the multilayer sample (3-4 layers) to 420 K, the spectrum (c) shows a single main peak (D, red) which is assigned to the equivalent nitrogen atoms of Cu-TPP. Further annealing to 490 K leads to a Cu-TPP monolayer (d).

molecule. Peak A with a binding energy (E_B) of 398.3 eV is assigned to iminic (=N-), peak B at E_B = 400.3 eV to pyrrolic (-NH-) nitrogen atoms. A third small peak C (E_B = 403.4 eV) is tentatively regarded to be a shake-up satellite following the argumentation in ref. 62. The assignment of the two main peaks is corroborated by former experimental results[62,63] and the results of our DFT calculations for the ionization potential of the iminic (E_{Calc} = 402.0 eV) and pyrrolic (E_{Calc} = 404.2 eV) nitrogen atoms in an isolated 2H-TPP molecule (Table I). Since molecule-surface interactions are not taken into account in the XPS and NEXAFS calculations the theoretically determined values and spectra are compared only to measurements of multilayers where it can be assumed that the substrate hardly has any direct influence on the molecules. While the calculated ionization potentials are referenced to the vacuum level the measured binding energies are referenced to the Fermi level which leads to an intrinsic difference of several eV between the respective values. The XPS calculations confirm that the binding energy of the pyrrolic nitrogen lies approximately 2 eV higher than that of the iminic nitrogen.

A 2H-TPP sample with an approximate coverage of slightly below one ML was prepared by evaporating free-base porphyrins onto the freshly cleaned copper surface. As our method of controlling the coverage is associated with a certain degree of uncertainty and it is necessary to avoid interfering signals from a possible second layer, the coverage of our prepared sample was chosen to be below one ML. The corresponding N1s XPS data (Fig. 2b) show two peaks that are assigned again to iminic and pyrrolic nitrogen species. A down-shift, i.e., a shift to lower binding energies, with respect to the multilayer sample is observed for both peaks. On a metallic substrate this is not unexpected and usually is explained by polarization screening effects.[32,40,64] In the 2H-TPP monolayer on Cu(111) the pyrrolic nitrogen peak shifts by a typical screening value of -0.5 eV. The iminic nitrogen, however,

shifts by only -0.1 eV which is a first indication that its chemical state is strongly affected by the adsorption. As a consequence the difference between the binding energies of the two nitrogen species is reduced to 1.6 eV (see section IV B for more details).

Not only the energetic peak splitting but also the ratio R of the peak area of the iminic divided by the pyrrolic nitrogen differs from the multilayer sample. Small intensity differences of the two nitrogen peaks have been reported before, though the values of R were much closer to one.[32,62,65] Here, instead of the expected value near to one, the pyrrolic peak dominates over the iminic. We found that this effect can be reproduced in a systematic way, i.e., that for a series with increasing coverage (from submonolayer to multilayer) R increases as well. Additionally, R depends not only on the thickness of the film but also on the angle under which the data are taken. Fig. 3 shows the N1s spectra of a 2H-TPP monolayer sample recorded for different angles between analyzer and sample. R is smallest (0.4) for the normal emission mode (Fig. 3b) and increases when the sample is rotated out of this position by angles of Δ = -25°(a), Δ = 10°(c) and Δ = 25°(d). In the latter position both peaks have nearly the same intensity.

We attribute this behavior to a photoelectron diffraction effect. Earlier work[66–68] revealed that for the kinetic energy and elements of our experiment forward scattering as well as backward scattering contribute substantially to the photoelectron signal intensities. Diffraction can only produce strong intensity variations if the electron emitting sources are surrounded by the same geometry of the scatterers. Therefore, we suggest that the iminic nitrogen atoms are pointing towards the surface with their lone-pair and are responsible for a well-defined adsorption place by optimizing their interaction with specific surface atoms. Similarly site-specific adsorption resulted from the nitrogen-surface interaction as shown in recent work.[52,69] Assuming photoelectron diffraction as the origin of the intensity vari-

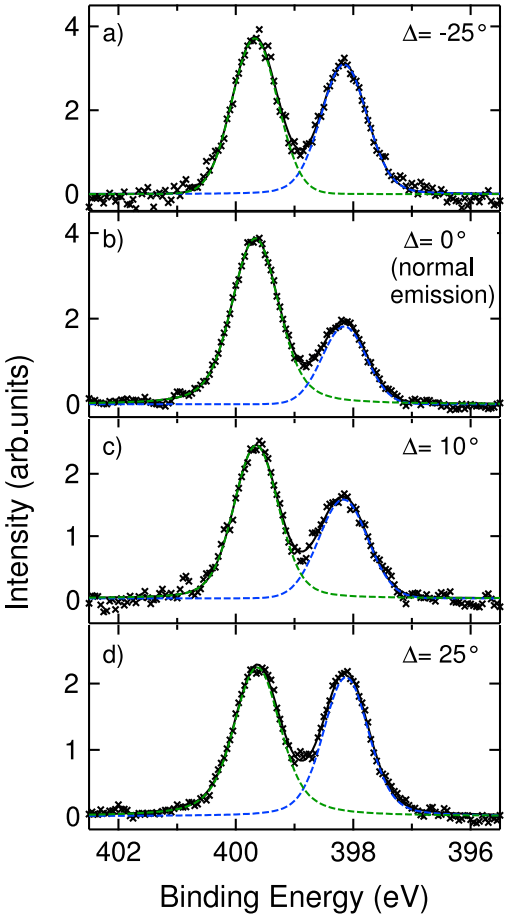

FIG. 3. The ratio of iminic (blue) and pyrrolic (green) N1s XPS peaks of a 2H-TPP monolayer is angular dependent. Whereas in the normal electron emission mode (b) the peak ratio is just 0.4 it increases when the sample is rotated out of this position by Δ = -25°(a), Δ = 10°(c) and Δ = 25°(d).

type	E_{exp}	E_{calc}	$\Delta E_{calc,exp}$
iminic (=N-)	398.3 eV	402.0 eV	3.7 eV
pyrrolic (-NH-)	400.3 eV	404.2 eV	3.9 eV
metalic (NCu)	398.8 eV	402.9 eV	4.1 eV

TABLE I. XPS energies of different nitrogen species obtained from multilayer measurements (E_{exp}) compared with calculated ionization energies (E_{calc}); nearly constant energy difference between experimental and theoretical results ($\Delta E_{calc,exp}$) for 2H-TPP (=N-, -NH-) and Cu-TPP (NCu).

ations would also account for the coverage dependence of R. At low molecular coverage every 2H-TPP is free to adopt the optimal adsorption place and geometry. With increasing coverage the molecules are pushed away from these positions. Consequently, the different scattering geometries around the nitrogen sources reduce the diffraction effects. Altogether, the peak positions and intensities indicate a strong interaction of the molecule with the substrate that is mediated primarily via the iminic nitrogen.

Next, we studied the change of the spectra induced by annealing. Fig. 2c shows a multilayer sample (approximately 3-4 layers) that has been heated to 420 K. The main feature is peak D at E_B = 398.8 eV with two shoulders at 398.0 eV and 399.9 eV. The total area of both C1s and N1s spectra remained nearly the same during the thermal treatment. After further annealing to 490 K (Fig. 2d) the relative intensity of the shoulders decreases and the position of the main peak shifts downward by 0.4 eV. The total intensity of the signal is less than in the multilayer suggesting a desorption of the multilayer molecules with a remaining monolayer. A very similar spectrum could be achieved by directly annealing monolayer and submonolayer samples to temperatures above 420 K.

The reduction of the two peaks of the inequivalent nitrogen species to one new main com-

ponent is an indication for the metalation of the 2H-TPP since metalloporphyrins possess four chemical equivalent nitrogen atoms generating only one N1s peak. The binding energy of the coordinated nitrogen peak in the multilayer (398.8 eV) is in accordance with that reported for directly sublimed Cu-TPP (398.9 eV)[62], Cu-TPP multilayers on gold (398.6 eV)[70] and is similar to the N1s binding energy of metalloporphyrin films like a Co-TPP monolayer on Ag(111) (398.8 eV)[34], a Zn-TPP monolayer on Ag(111) (398.7 eV)[33] and a Fe-TPP multilayer on Ag(111) (398.6 eV)[32]. Our calculations for the isolated Cu-TPP predict an ionization energy that lies 1.3 eV below the energy of the pyrrolic nitrogen, i.e., a binding energy of 399.0 eV, assuming the same work function for 2H-TPP and Cu-TPP. Our experimental value of 398.8 eV lies only 0.2 eV lower, confirming the assignment. Comparable to the 2H-TPP spectra the N1s signal for the Cu-TPP shows a down-shift of 0.4 eV when proceeding from multi- to monolayers which is attributed to screening and suggest a weakly chemisorbed macrocycle. The low-energy shoulder in the annealed multilayer spectrum (Fig. 2c, black dashed peak at E_B = 398.1 eV) most likely mainly originates from the downshifted signal of the monolayer but may also include intensity from residual, not metalated porphyrins.

The XPS results alone are not fully conclusive for the metalation as a deprotonation of the pyrrolic nitrogen groups upon annealing potentially also leads to the formation of a single N1s peak. Even though in three-dimensional environments a formally doubly negative radical is extremely unlikely, on the surface deprotonated species can be stabilized via the special interface conditions at the metal substrate.[71–74] Additional evidence for the formation of Cu-TPP is therefore provided by comparing N and C K-edge NEXAFS spectra of 2H-TPP films with annealed 2H-TPP layers. The angle resolved nitrogen edge spectra are displayed in Fig. 4, the carbon spectra in Fig. 5, respectively. The comparison of multi- and monolayers

reveals substantial changes in the N1s region (Fig. 4a vs. 4b and 4c vs. 4d) as well as in the C1s region (Fig. 5a vs. 5b and 5c vs. 5d) suggesting a strong influence of the substrate that leads to electronical and conformational changes, which will be discussed in detail in section IV B. At this point we want to focus on the self-metalation and therefore consider only the multilayer spectra (Fig. 4a and 4c, Fig. 5a and 5c).

The N K-edge π^* region of the 2H-TPP multilayer shows an isolated resonance (Fig. 4a, peak A) at 397.6 eV, followed by four peaks (B-E) lying between 399.8 eV and 403.6 eV and a σ^* region (405-415 eV) with broad structures. All resonances exhibit very similar angular dependencies. The general structure of the data agrees well with others reported for 2H-TPP[32,35,45] which confirms the intactness of the molecules. Annealing of a 2H-TPP multilayer leads to essential changes in the nitrogen spectra (Fig. 4c). A single resonance at low excitation energies (399.1 eV) is still present, but compared with the freshly prepared multilayer curves its position is shifted by 1.5 eV to higher photon energies. The number of peaks in the following structure of the π^* region is reduced from four (peaks B-E) to two. Again, the angular dependencies of the various peaks in Fig. 4c are very similar. Peak structure and positions of Fig. 4c are typical for metalloporphyrins in general[32,43,45] and Cu-TPP in particular,[75] which gives further evidence for the metalation of the free-base porphyrin.

The NEXAFS C K-edge π^* region of the 2H-TPP multilayer (Fig. 5a) exhibits six peaks. Peak F at 284.2 eV is followed by two dominant peaks at 285.0 eV (G) and 285.4 eV (H). The adjacent features I-K are not easily separable without fitting. Contrary to the nitrogen spectra the resonances in the carbon region show different angular behavior: peaks G and K become stronger with the angle θ increasing, while peaks F and J become weaker (cf. section IV B). After annealing the multilayer sample to 420 K the position as well as the number

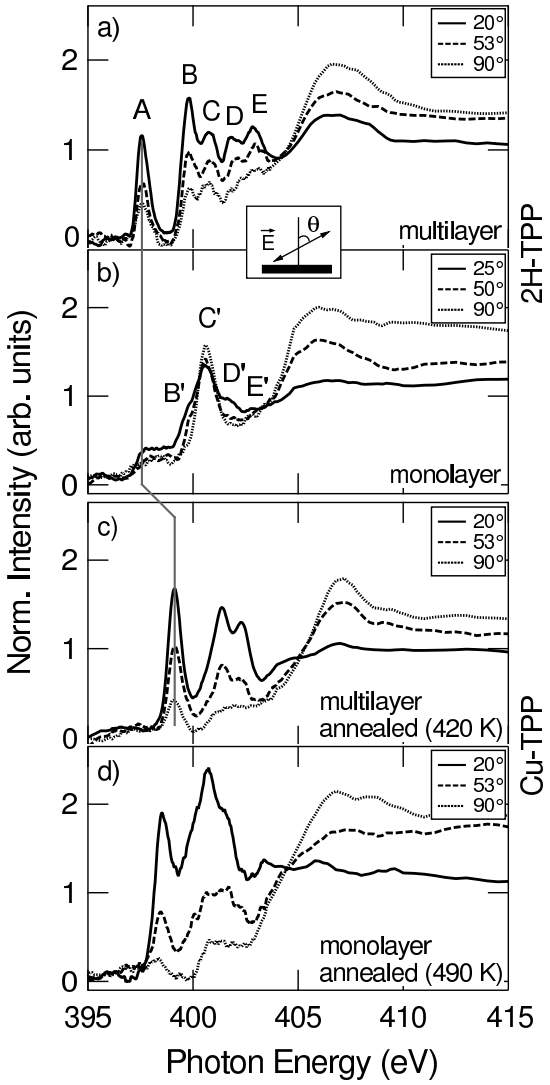

FIG. 4. Comparing N K-edge NEXAFS spectra of (a) a 2H-TPP multilayer and (b) a 2H-TPP monolayer shows the big influence of the surface on the molecule. After annealing both the multilayer (heating to 420 K, c) and the monolayer (heating to 490 K, d) signatures are different from the 2H-TPP spectra and indicate the metalation to Cu-TPP. Values in the insets denote the incident angle θ.

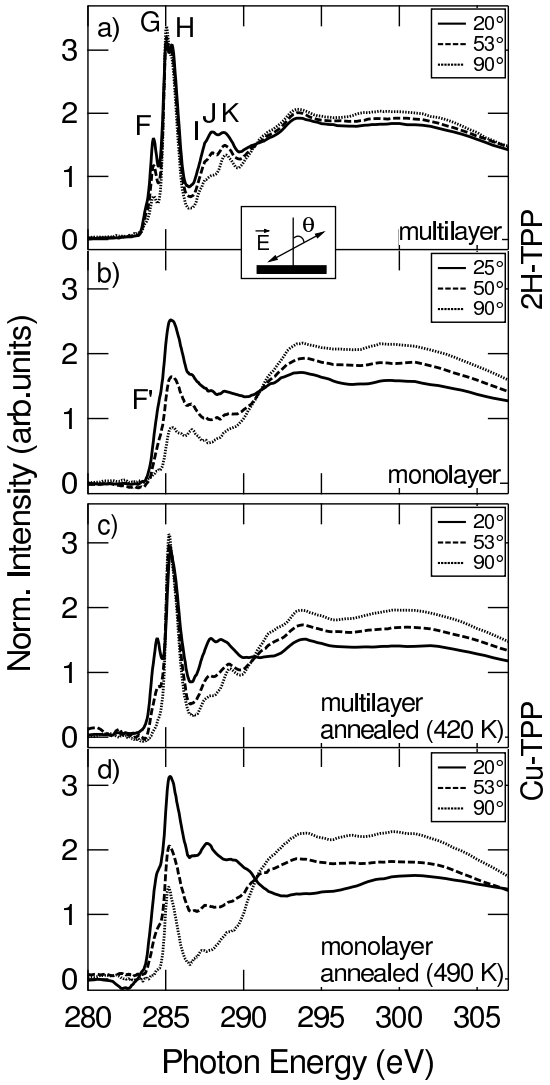

FIG. 5. The differences of the C K-edge NEXAFS spectra between (a) a 2H-TPP multi- and (b) a 2H-TPP monolayer as well as between the annealed multi- (c) and monolayer (d) show the influence of the surface on conformation and electronic structure of the molecules. Values in the insets denote the incident angle θ.

of peaks remain nearly unchanged (Fig. 5c), only the angle-dependencies of peaks F and H differ from that in the 2H-TPP multilayer signal. The changes in the carbon structure are therefore dominated rather by conformational than by chemical effects, contrary to the changes to the nitrogen data.

The experimental results were compared with simulated NEXAFS gas phase spectra of isolated 2H-TPP and Cu-TPP molecules. Fig. 6 compares the experimental magic angle (53°) multilayer curves (top) with the calculated data (middle, bottom). As the differences between the measured spectra of 2H-TPP and annealed films are mostly related to the nitrogen atoms we focus at this point only on the N K-edge curves and discuss the C K-edge together with the changes in section IV B. The total simulated spectrum of 2H-TPP (Fig. 6b, middle) consists of the sum of two spectra with varying excitation center, the iminic (bottom panel, dashed blue line) and pyrrolic (bottom panel, solid green line) nitrogen species. The good agreement between experiment and simulation allows the assignment of the 2H-TPP peaks (cf. section IV B) and shows that the identification of a molecule is possible with this method of combining experimental and theoretical results.

In Fig. 6c the experimental 53°-spectrum of the annealed multilayer (top panel) is compared with the simulated spectrum for the excitation of a coordinated nitrogen atom in the Cu-TPP molecule (middle panel). Spectrum 6d shows the calculated N K-edge spectrum of a dehydrated 2H-TPP (denoted as TPP). At this point, even without a detailed peak analysis (which will follow in section IV B), the similarities in shape and position of the experimental data with the peak structure of Cu-TPP and the discrepancy to that of the TPP rule out a possible temperature-induced dehydration in favor of the self-metalation.

The in situ metalation of adsorbed porphyrins with on top deposited metal-atoms has been reported for Fe, Co, Ni and Zn atoms.[30–35] The metalation of 2H-TPP with vapor-

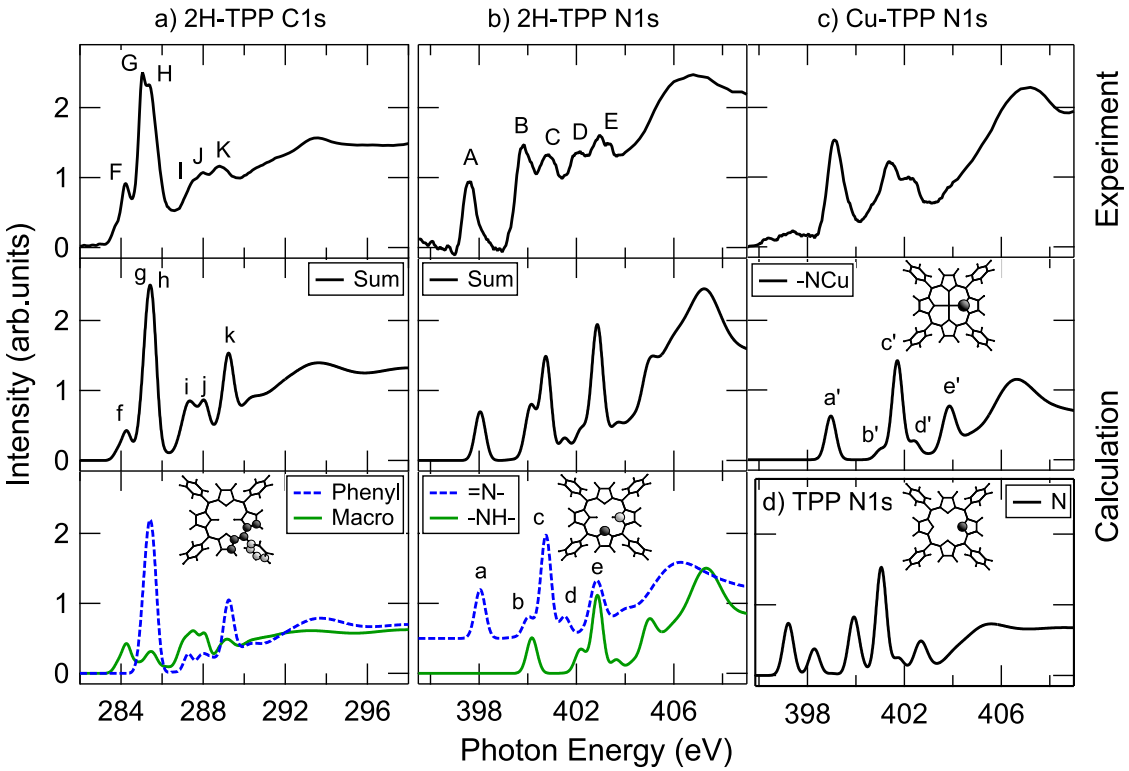

FIG. 6. Comparison of experimental (top) and calculated (middle, bottom) NEXAFS spectra for the C-edge 2H-TPP multilayer spectrum (a), the N-edge 2H-TPP multilayer spectrum (b) and the N-edge Cu-TPP multilayer spectrum (c). (d) shows the calculated N-edge TPP spectrum. The middle panel displays the sum of all corresponding single spectra, in the bottom panel this total spectrum is split up into its single components. The insets show the position and number of the atoms used for the calculation of the respective spectra.

deposited Zn atoms requires annealing to at least 510 K[33], while the reaction of Fe, Co or Ni atoms with predeposited porphyrin films already takes place at room temperature[30,34,35]. DFT calculations predict a lower activation barrier for Cu than for Zn[33] which is in accordance with our observations as temperatures of at least 420 K were required for the self-metalation process.

The incorporation of Cu atoms into the porphyrin macrocycle either requires the presence of a significant amount of adatoms on the terraces or the removal of copper atoms from the topmost substrate layer. For the Cu(111) facet the adatom-vacancy formation energy was calculated to be approximately 2 eV[76,77] while the adatom detachment from kinks requires only 0.76 eV[78]. Mass exchange with the terraces by adatom extraction sets in at 500 K and is already at 600 K the dominant mass transport mechanism.[78,79] The exchange leads to a surface gas with a coverage of typically several percent of a ML in this temperature range.[80] In our case metalation takes place at 420 K, which is a smaller temperature as compared with the values above. We suggest that the presence of the organic species, already mobile at that temperature leads to a reduction of the detachment barrier and attribute the metalation to the incorporation of adatoms of the surface gas. Consistently, a recent work explained the formation of metal-organic networks at 420 K on the same surface with the incorporation of the surface gas adatoms.[81] Likewise, González-Moreno et al. conclude that a high density of adatoms is one of the factors which enable the self-metalation of 2HPPIX on Cu(110) and Cu(100) at room temperature.[38] Compared with the detachment of adatoms the extraction of an atom from the topmost layer of the Cu(111) surface is energetically more costly. Nevertheless, we cannot rule out this mechanism completely as the formation energy of Cu-TPP (cf. Supporting Information of ref. 33) seems to be sufficiently high to permit the extraction of a surface atom, in particular given that it is possible that the presence

of a strongly interacting porphyrin can reduce the necessary energy barrier. A very recent publication by Doyle et al. backs this scenario.[82]

So far metalation processes were typically shown for monolayers of free-base porphyrins though in few cases also multilayers were metalated.[32,83] Our data show that self-metalation is possible for films whose thicknesses exceed one monolayer which raises the question of the transport mechanism involved. Three scenarios seem reasonable: The first is that the metalation only takes place directly on the surface and diffusion of the metalated porphyrins within the film leads to several layers of Cu-TPP. In the second scenario neither free-base nor metalloporphyrins are mobile but metalation happens in channels consisting of stacked macrocycles. The first layer of 2H-TPP is metalated by the substrate. All other free-base porphyrin layers are metalated by receiving copper atoms from the already metalated Cu-TPP layer underneath. Another possibility is the diffusion of copper atoms from the substrate into the porphyrin film, subsequently the metalation takes place both at the porphyrin-copper interface and within the film. To our knowledge the metalation of porphyrin multilayers so far has been done by evaporating metal atoms on top of the predeposited molecules[32,83] which leads to a diffusion of the metal atoms into the film.[83] The opposite case, a diffusion of copper atoms from the substrate into a film of on-top deposited organic molecules is reported in ref. 84. From our data it is not possible to conclude which of the scenarios is correct, however, interdiffusion of either molecules or copper atoms seems more likely than metalation through porphyrin channels because of the rather high formation energy of Cu-TPP (ref. 33, Supporting Information).

B. Molecular conformation and electronic structure

The conformation of metalated and non-metalated films, i.e., mono- and multilayers of 2H-TPP and Cu-TPP were investigated by using angle-resolved NEXAFS measurements. NEXAFS allows to probe the unoccupied states and to obtain information on the conformation of the adsorbed molecules. Our analysis focuses on the interpretation of the π^* region as the decomposition of the broad σ^* region in single excitations is less feasible. For aromatic groups the π^* states consist of p_z orbitals that lie perpendicular to the plane of the aromatic structure. Their NEXAFS signatures depend on the incidence angle θ, i.e., the angle between the linear polarization of the light and the surface normal. In this study all spectra were taken for three incidence angles (cf. Fig. 4 and Fig. 5). For an aromatic π^* system lying coplanar to the substrate the corresponding peaks theoretically should be maximal for $\theta = 0$ and minimal for $\theta = 90°$.[46] According to the building-block principle the spectrum of a molecule composed of several subgroups can be divided in the signatures of the subgroups as long as the corresponding orbitals are independent from each other.[46] Thus, the assignment of the peaks in the measured NEXAFS spectra to the subgroups of the molecule is crucial for the determination of the molecule's conformation with respect to the surface. Although the multilayer spectra already have been briefly discussed in section IV A the peak assignment and discussion of the angle-dependency have yet to be done.

Below 404 eV the N K-edge π^* region of the 2H-TPP multilayer (Fig. 4a) shows five main peaks (A-E) with very similar angular dependencies. The intensity of all peaks decreases with increasing incidence angle. The peak assignment and determination of the conformation will be based on results of the DFT calculations.

The simulated NEXAFS N K-edge spectra (Fig. 6b, middle and bottom panel) are com-

pared with the experimental curve (Fig. 6b, top panel) taken at the "magic angle" as the calculation assumes a gas phase configuration, i.e., no specific direction of the polarized light is taken into account. The theoretical 2H-TPP spectrum (Fig. 6b, middle) is a superposition of the curves of the iminic (Fig. 6b, bottom, blue dashed line) and the pyrrolic (Fig. 6b, bottom, green straight line) nitrogen species. The spectrum of the iminic nitrogen is shifted upward in intensity in order to better see the structure of both curves. The calculations were performed for all four nitrogen atoms without symmetry constraints. Spectra and energies were nearly identically for the two respective kind of nitrogen atoms, thus the displayed two spectra contain all information. In the inset of Fig. 6b the two excitation centers are indicated by a light (pyrrolic) and a dark (iminic) sphere, respectively. The spectrum of the iminic nitrogen atom shows a four-peak structure below the ionization energy, starting with a single transition (peak a) followed by three peaks with alternating intensities (low-high-low, peaks b-d). This structure is followed by a single peak (peak e) whose energy lies over the ionization threshold. The pyrrolic nitrogen shows a similar signature that is shifted upwards by 2.1 eV which is originating from the energy splitting of the N1s core levels according to our calculations.

In each spectrum the first peak consists of a single transition to the LUMO, while the following peaks consist of a multitude of transitions. A detailed listing of the main contributions to the spectral features is given in Table II. The alikeness of the pyrrolic and iminic nitrogen spectra can be understood by looking at shape and energy of the excited unoccupied orbitals which are similar for the excitation of the two different nitrogen atoms. In Fig. 7 the final state orbitals (of the transition potential calculation) of the four strongest π^* transitions as well as the LUMO+1 are displayed. The LUMO is located mainly at the macrocycle with non-vanishing components at the respective excitation center which explains the very

TABLE II. Peak assignment for the N1s peaks in the 2H-TPP NEXAFS spectrum, only main transitions below the ionization energies are listed

Peak[a]	Experimental[b](eV)	Computed[c](eV)	Strength[d]	Exc. Center[e]	Transition[f]
A	397.6	398.04	vs	=N-	1. (1s) → 159. (LUMO)
		399.98	s	=N-	1. (1s) → 162. (LUMO+3)
B	399.8	400.03	w	=N-	1. (1s) → 163. (LUMO+4)
		400.17	vs	-NH-	1. (1s) → 159. (LUMO)
		400.19	w	=N-	1. (1s) → 168. (LUMO+9)
C	400.7	400.74	vs	=N-	1. (1s) → 170. (LUMO+11)
		402.12	s	-NH-	1. (1s) → 162. (LUMO+3)
D	401.6-402.3	402.20	w	-NH-	1. (1s) → 163. (LUMO+4)
		402.34	w	-NH-	1. (1s) → 167. (LUMO+8)
		402.86	vs	-NH-	1. (1s) → 170. (LUMO+11)
E	402.6-403.6	403.62	s	-NH-	1. (1s) → 177. (LUMO+18)
		404.12	w	-NH-	1. (1s) → 185. (LUMO+26)

[a]Peaks in experimental spectra (cf. Fig. 4)

[b]Experimental peak positions (as measured)

[c]Computated peak positions (shifted by -0.9 eV to match experimental spectrum)

[d]Oscillation strengths: vs: very strong (> 0.001), s: strong (0.0005-0.001), w: weak (0.0001-0.0005)

[e]Excitation center: $n = 0.5$ in transition state calculation

[f]Transition (orbital numbers), final state orbitals for strong and very strong transitions are displayed in Fig. 7

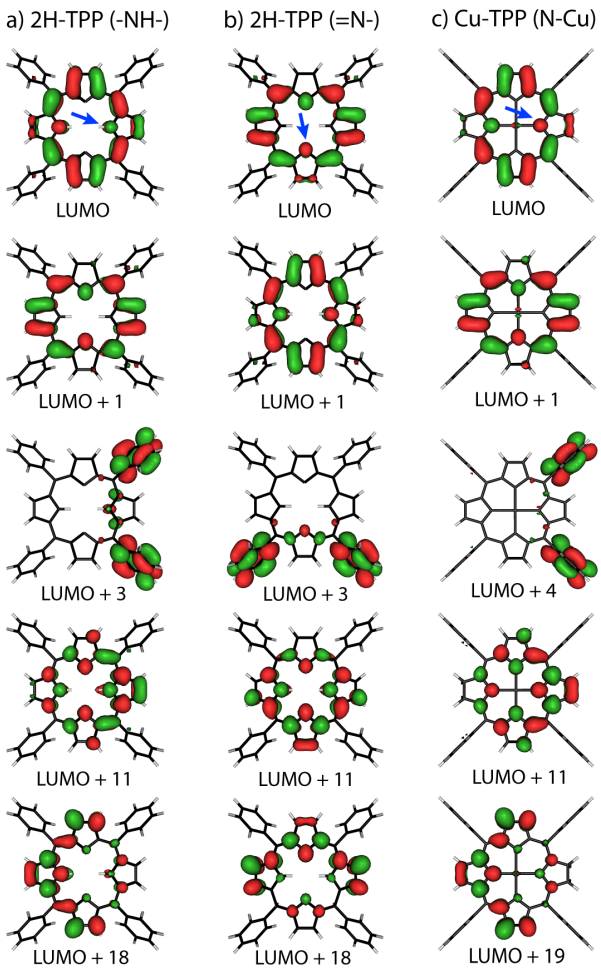

FIG. 7. Molecular orbitals obtained from transition state calculations; (a, b) 2H-TPP, (c) Cu-TPP, excitation centers are marked by an arrow

strong oscillation strength for this transition. The LUMO+1 has a similar shape, although the main contributions are located not at the excitation center but at the other nitrogen species. The missing overlap with the N1s orbital of the excitation center results in values close to zero for the respective element of the transition matrix. The simulated orbitals are consistent with those in recently reported DFT calculations on 2H-TPP.[45,85]

The comparison of the simulated and the experimental spectrum at this point already allows a peak assignment for the nitrogen region of the measured data (table II). A closer analysis is done by applying the information from the calculations to the fitting of the experimental spectra. In Fig. 8a we show in an exemplary case how the nitrogen curves of the 2H-TPP multilayer (cf. Fig. 4a) were fitted using three sets of Gaussian peaks. Two sets represent the iminic and the pyrrolic nitrogen species, the third an additional background accounting for the increase of the adsorption intensity around the ionization energy.[46] Each of the two nitrogen sets consisted of four peaks modeling the simulated spectra with a single peak at lower energies (peak a) followed by a triple peak structure (peaks b-d). Within each set the intensities of the single peaks have to follow the same angular dependence and energies and widths were kept at fixed values relative to the first peak. Thus, the fitting procedure only optimizes three independent parameters for the reproduction of the whole π^* range. Fig. 8a shows the result of the fit for the 53° curves. The experimental data points (symbols) are well represented by the total fit (straight red line) which is a sum of the iminic (dashed blue line), the pyrrolic (dotted green line) and the background (dashed-dotted cyan line) sets. For obtaining such a good overall agreement only slight changes to the calculated peak parameters had to be introduced in the modeling of the nitrogen sets. In Fig. 8b the analysis of the angle-dependence of the multilayer N-edge is presented. The normalized intensities obtained by fitting the whole series (symbols) are compared with

curves that show the theoretically expected dependency of the normalized intensities on the incidence angle θ for several angles α between the π-type resonance and the surface normal (cf. inset in Fig. 8b) assuming a threefold symmetry of the surface (black curves) that needs to be taken into account to cover the possibility that the molecules are rotated by different azimuth angles. The measured NEXAFS curve is an average of the signals from differently orientated molecules. Our assumption that the azimuthal orientation of the adsorbed 2H-TPP molecules follows the threefold symmetry of the surface is corroborated by STM studies of 2H-TPP on Cu(111). At 77 K[85] as well as at room temperature[86] the molecules adsorb in only three different azimuthal orientations, following the symmetry of the surface. The values indicate a tilt of 40° for both kind of pyrrol rings (with and without hydrogen) of the macrocycle.

The π region of the C K-edge multilayer spectrum of 2H-TPP (Fig. 5a) shows five main peaks with different angular dependencies (peaks F-K). The comparison with the C-edge NEXAFS spectra of benzene[87] and Zn-OEP[39] suggests that the measured curves can, according to the building block principle, be deconvoluted in one part originating from the carbon atoms of the macrocycle and another one coming from the phenyl rings. To verify this assumption DFT calculations were performed for one phenyl ring and the corresponding part of the macrocycle (Fig. 6a, inset) assuming a fourfold symmetry of the molecule. The results for the macrocycle (continuous green line) and the phenyl rings (dashed blue line) are exhibited in the bottom panel of Fig. 6a, their sum is displayed in the middle panel where it can be directly compared with the experimental 53° curve in the top panel. Generally, the calculated data are well reproducing all the main peaks of the measured curves. Both spectra are dominated by two main features (G/H and g/h, respectively), whose splitting is more dominant for the experimental (peaks G at 285.0 eV and H at 285.4 eV) than

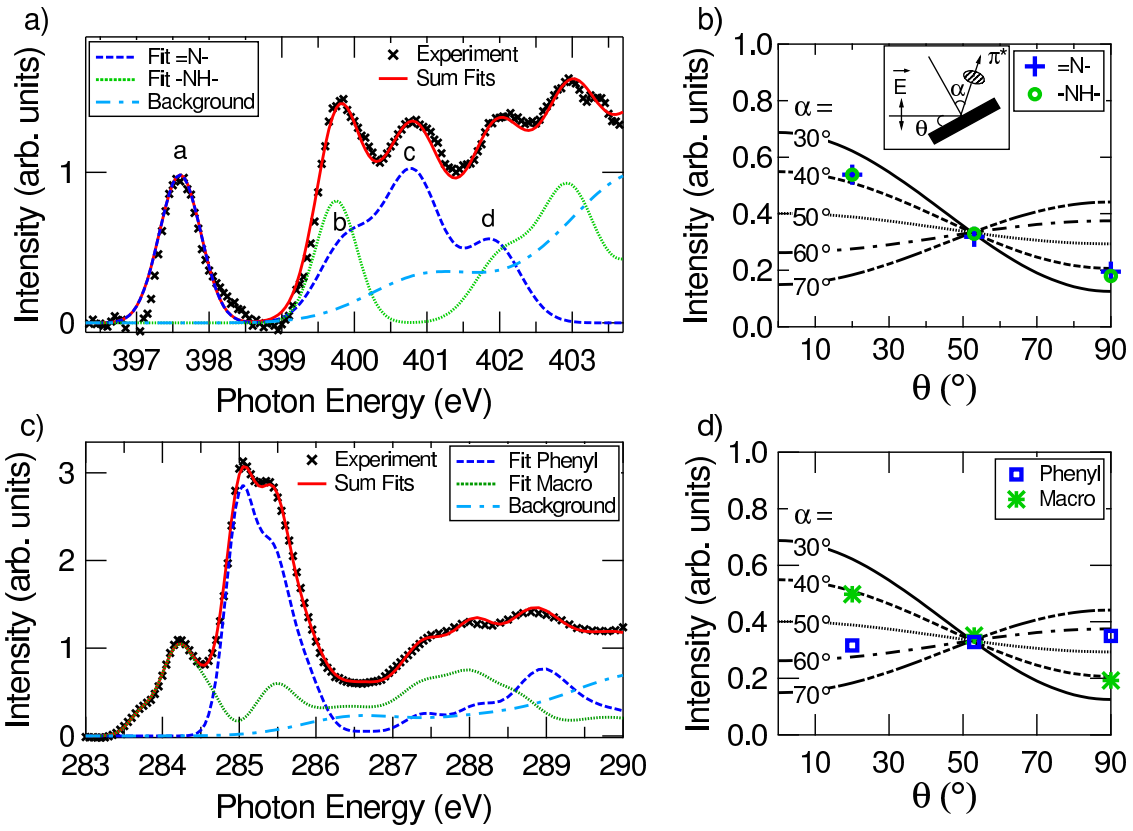

FIG. 8. Fits for the experimental multilayer N-edge (a) and C-edge (c) region (for clarity only the 53° curves are shown). The good agreement of the sum (red continuous line) of all single fits (dashed and dotted lines) with the experimental data (symbols) allows to determine the conformation of the molecules. Therefore the dependence on the incidence angle θ of the normalized intensities (symbols) obtained from the fit are compared with the theoretical curves of a π system on a threefold symmetric surface (black curves, b and d). The curves for different angles α between orbital and surface normal assumed a linear polarization of 0.9. The inset in (b) illustrates the angles involved in the measurement and analysis. The circle symbolizes the conjugated system which is coplanar to the surface for $\alpha = 0$.

for the theoretical data. As well, peak F at 284.2 eV and peaks I-K at higher photon energies have direct counterparts in the simulated spectrum (peaks f and i-k, respectively). Taking into account the deconvolution of the computated spectrum in two parts originating from the macrocycle and the phenyl rings (Fig. 6a, bottom) it becomes clear that peak F can be assigned completely to the macrocycle signal while peaks G and H are mainly originating from the phenyl rings with small contributions from the macrocycle which is in good agreement with NEXAFS data of porphyrins without meso-substituents.[39,88] For them and the other peaks which are a superposition of signals originating from both parts the total angular behavior depends on the relative intensities of the contributing resonances. As a test of our theoretical description of the carbon edge, the same fitting procedure as was described for the N region has been applied for the analysis of the C region. Again the differences between the calculated peak parameters and the ones necessary for a good fit agreement are small. For example the intensities of peaks I, J and K of the experimental curve are similar while peak k of the calculated spectrum is nearly twice as high as peaks i and j. The same trend was observed for TD-DFT calculations of 2H-TPP.[45] The analysis of the angular dependencies (Fig. 8d) indicate an angle of $\alpha_{mac} = 40°$ for the orientation of the macrocycle and an angle of $\alpha_{ph} = 55°$-$60°$ for the tilt of the phenyl rings. We assume that α_{ph} is exclusively related to the rotation of the phenyl groups (cf. Fig. 1) without an additional tilt of the whole subgroup out of the molecular plane. The value of α_{mac} describes an average of the signal of the two different kind of pyrroles in the macrocycle. α_{mac} is used to corroborate the information obtained from the fit of the nitrogen curves as a further disentanglement of the carbon signal is not reasonable. The two values for the macrocycle orientation obtained from the C and the N edge agree well and confirm the validity of our analysis.

It has to be pointed out that in the multilayer case it is nontrivial to relate the determined angles to the conformation of the molecules since the overall orientation of the molecule in the film is unknown. The determined value only describes the angle between the π system and the surface normal, but does not differentiate whether it originates from a deformation of a molecule whose macrocycle plane is parallel to the surface or from a tilt of the whole porphyrin. Nonetheless the fits affirm the validity of the peak assignment based on the results of the calculations. For both regions the overall shape of experimental and simulated spectra are consistent even though the relative intensities of the peaks fit only qualitatively and not quantitatively.

The 2H-TPP monolayer spectra of the nitrogen (Fig. 4b) as well as of the carbon (Fig. 5b) region differ greatly from those of the multilayer. Generally all peaks appear broadened. This increase of the peak width can be explained by shorter lifetimes of the excited states caused by fast charge transfer between substrate and molecules. Although the broadening complicates the comparison between the individual peaks of multi- and monolayer spectra several differences are evident. In the N K-edge spectra (Fig. 4b) the first transition of the multilayer spectrum (peak A) is missing completely. This resonance was assigned to the transition from the 1s orbital to the LUMO of the iminic nitrogen atoms. Its quenching in the monolayer spectra indicates a static electron charge transfer from the substrate to the LUMO during adsorption. This is well conform with recent publications by Tseng et al. who also correlate the absence of the first resonance to a filling of the LUMO[89] and by Rojas et al. who report on a charge transfer from the copper surface to the thereon adsorbed 2H-TPP molecules[85]. Instead of this quenched resonance a step is observed which does not show any significant angular dependence. This, as well as the fact that the step is very broad (2 eV) suggests that it is not composed of resonances from molecular orbitals but stems

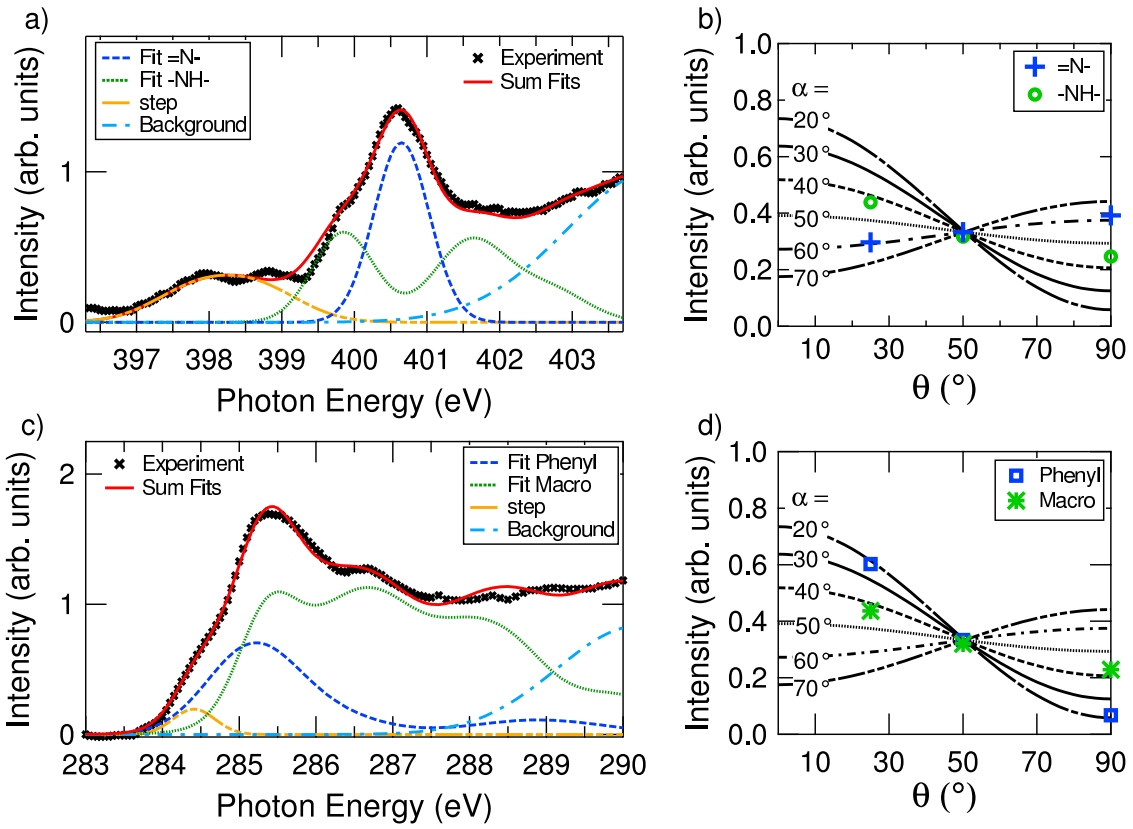

FIG. 9. Fits for the experimental 50° curves N-edge (a) and C-edge (c) region of a 2H-TPP monolayer lead to the analysis of the normalized intensities (b, d) which indicates a substantial distortion of the macrocycle. The theoretical curves (black curves, b and d) assumed a threefold symmetric surface and a linear polarization of 0.82.

from the substrate. This feature possibly could originate from the strong coordination of the nitrogen to the substrate, so that transitions to unoccupied metal-adsorbate-states are possible.[90] Such states typically are characterized by a negligible angle-dependence of their intensity, corresponding well with our findings. Furthermore, compared with the multilayer the nitrogen spectra of the monolayer exhibit a noticeably different angular dependence. The spectra show one main peak (peak C') that corresponds to peak C in the multilayer spectra, while peaks B', D' and E' are part of the broad structure around the main peak and do not appear as clear single peaks. For a quantitative analysis again a fitting procedure was applied to the three monolayer curves, this time with peak parameters more freely chosen to optimize the fit agreement. As peak C was completely assigned to resonances of the iminic nitrogen (Fig. 8a) it seems reasonable that for peak C' the same is valid. It was found that indeed the best fit was obtained for the assumption that peak C' completely arises from the excitation of the iminic nitrogen species while the rest of the peaks are assigned to pyrrolic nitrogen resonances and the θ independent step at 398 eV to an additional background (Fig. 9a). This fit gives an estimation for the tilting angles of the macrocycle: $\alpha_{imi} = 60°$ for the iminic and $\alpha_{pyrr} = 40°$ for the pyrrolic nitrogen (Fig. 9b).

In the same way the carbon region is analyzed. Compared with the multilayer curves (Fig. 5a and Fig. 8c) the intensities of the first resonances (which were assigned to macrocycle excitations in the LUMO) of the monolayer spectrum (Fig. 5b and Fig. 9c) are reduced or disappear completely which supports the conclusion from the N-edge analysis that an electron transfer from the substrate to the adsorbed molecule occurs. As the remaining structure is very broad and the peaks are smeared out the fit of the carbon region turns out to be difficult. However, it is possible to find a reasonable fit that maintains the general shape (though with broadened peaks) of the part associated with the resonances of the

	2H-TPP			Cu-TPP	
	α_{imi}	α_{pyrr}	α_{ph}	α_{coord}	α_{ph}
multilayer	40°	40°	55-60°	20-30°	60°
monolayer	60°	40°	20°	10-20°	40-50°

TABLE III. Angles derived from NEXAFS measurements of mono- and multilayers of 2H-TPP and annealed 2H-TPP (Cu-TPP) samples. α_{imi}, α_{pyrr} and α_{coord} describe the inclination of the pyrrole rings out of the macrocycle plane, whereas α_{ph} refers to the rotation of the phenyl rings (see Fig. 1). To interpret the angles in terms of adsorption geometry further information has to be taken into account (see text).

phenyl rings while the main changes happen in the remaining structure connected to the macrocycle excitations (Fig. 9c). As with the nitrogen region the best fit is obtained for vanishing first macrocycle resonances which are replaced by a (smaller) step not showing any angular dependence (Fig. 9c, orange). For the macrocycle the fitting procedures give an angle of $\alpha_{mac} = 40°$ while the angle related to the phenyl rings is $\alpha_{ph} = 20°$(Fig. 9c and d). Mono- and Multilayer angles are displayed in Table III.

Due to the problem with the fits of the broadened structures the exact values of the angles may differ from those given here, nevertheless the general trends are certainly reasonably well reproduced. It has to be pointed out that the NEXAFS results alone are not fully sufficient to propose a conformational model of the 2H-TPP on the Cu(111) surface, as it is not possible to determine whether the pyrrole and phenyl rings point up or down. Taking into account former STM results of adsorbed porphyrins[29,40,52,91] as well as calculations on the conformation of porphyrins[45,92], our data suggest a saddle-shaped conformation where the iminic nitrogen atoms point towards the surface (α_{imi} = -60°, the negative sign is used

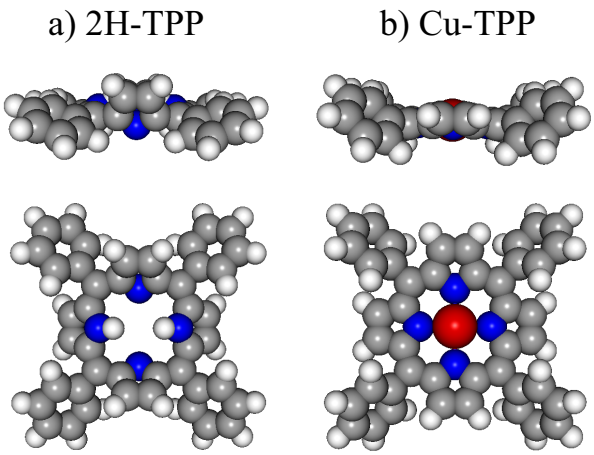

FIG. 10. ide and top view model of a) a free-base porphyrin with a marked saddle-shaped conformation, where the iminic nitrogen atoms are pointing downwards, i.e., with the nitrogen lone pair towards the substrate and the pyrrolic nitrogen atoms are pointing upwards and b) a slightly saddle-shaped Cu-TPP conformer with a nearly flat macrocycle (for the atoms the same color code as in Fig. 1 is used).

to emphasize the orientation towards the surface) and the pyrrolic nitrogen atoms point upwards ($\alpha_{pyrr} = 40°$). Generally the phenyl rings of a saddle-shaped tetraphenylporphyrin are pairwise rotated out of the macrocycle plane by an angle α_{ph}. Contrary to the multilayer, where the determined angle of $\alpha_{ph} = 55°$-$60°$ is in good agreement with the angles determined by ab initio calculations[93] of a tetraphenylporphyrin in gas phase ($\alpha_{ph} = 63°$) and by STM of porphyrins adsorbed on Ag(111)[94,95], the strong distortion of the macrocycle allows a rather flat orientation of the phenyl rings ($\alpha_{ph} = 20°$). The adsorption geometry of the saddle-shaped free-base porphyrin in the monolayer is depicted in Fig.10a.

At this point, it is instructive to discuss the interaction between the copper surface and the iminic nitrogen as indicated by the combined data of XPS and NEXAFS. In XPS the increase of electronic density in the surrounding of an excitation center leads to a shift to lower binding energies. Thus, with the iminic nitrogen near to the surface and a filling of the LUMO, one would expect a pronounced downshift of the iminic signal (peak A, Fig. 2) during adsorption. Instead a rather weak downshift appears. As explanation, we propose a charge donation-backdonation process similar to the one discussed in ref. 6. The backdonation reduces the electron density in the vicinity of the iminic nitrogens by an emptying of lower-lying σ-orbitals. An alternative explanation could be the formation of an intermediate complex in which the H atoms are still present and the N are only partially bonding to the Cu atom, which was suggested by Doyle et al. in reference 82. However, this situation is not consistent with our NEXAFS data which show a broad, nearly angle-independent step-like feature instead of the reported resonance at 398.8 eV and thus is ruled out.

Now we proceed with the analysis of the Cu-TPP mono- and multilayer samples. It has been reported that the differences between the NEXAFS spectra of 2H-TPP on the one hand and Zn-TPP and Co-TPP on the other hand are much more prominent in the nitrogen than

TABLE IV. Peak assignment for the N1s peaks in the Cu-TPP NEXAFS spectrum, only main transitions below the ionization energies are listed

Experimental[a](eV)	Computed[b](eV)	Strength[c]	Transition[d]
399.1	398.97	vs	1. (1s) → 173. (LUMO)
	400.96	w	1. (1s) → 176. (LUMO+3)
400.3-400.9	401.00	w	1. (1s) → 177. (LUMO+4)
	401.13	w	1. (1s) → 181. (LUMO+8)
401.4	401.71	vs	1. (1s) → 184. (LUMO+11)
	401.72	w	1. (1s) → 185. (LUMO+12)
	402.30	w	1. (1s) → 190. (LUMO+17)
402.3	402.42	s	1. (1s) → 192. (LUMO+19)
	402.53	w	1. (1s) → 193. (LUMO+20)

[a]Experimental peak positions (as measured)

[b]Computated peak positions (shifted by -0.9 eV to match experimental spectrum)

[c]Oscillation strengths: vs: very strong (> 0.001), s: strong (0.0005-0.001), w: weak (0.0001-0.0005)

[d]Transition (orbital numbers), important final state orbitals are displayed in Fig. 7

in the carbon region.[45] We found this to be true also for 2H-TPP and Cu-TPP. The C K-edge spectra of our 2H-TPP multilayer before (Fig. 5a) and after annealing to 420 K (Fig. 5c) are very similar, only peaks F and H show a different angular dependence. This indicates

that changes upon annealing are mainly related to the carbon atoms in the macrocycle, whereas the phenyl rings are not affected. In agreement with this assumption are the marked changes in the nitrogen multilayer between the 2H-TPP (Fig. 4a) and the Cu-TPP (Fig. 4c) multilayer. The first resonance (peak A') is shifted upwards and the number of peaks is reduced, which is expected for the coordinated molecule with only one nitrogen species.

Both the simulated NEXAFS N-edge of an isolated Cu-TPP molecule (Fig. 6c, middle) and the experimental 53° curve (Fig. 6c, top) show four resonances in the π^* region (398-403 eV). A well-separated transition (peak a') at 399.0 eV is followed by a threefold structure with a low-high-low intensity profile (peaks b'-d'). Similar to 2H-TPP the intensity of peak c' is overestimated by the calculation. The calculated peak e' at 403.9 eV has no directly visible counterpart in the experimental data. It lies close to the ionization threshold where the applied broadening may be to small compared with the smeared resonances of the experiment. The shapes of the Cu-TPP final state orbitals resemble those of the excited 2H-TPP molecule (Fig. 7) which is an explanation for the similarity of the single nitrogen spectra. Like for the free-base TPP the first resonance (peak a') is associated with the transition to the LUMO of the excited molecule. An assignment of the main transitions is given in table IV.

The fit of the nitrogen spectra give an angle of $\alpha_{coord} = 30°$ for the pyrrole rings of the Cu-TPP multilayer while the fit of the carbon spectra give an angle of $\alpha_{ph} = 60°$ for the phenyl rings and $\alpha_{mac} = 20°$-$30°$ for the macrocycle.

As the angles determined from the multilayer are not necessarily related to the conformation of the molecule, but can also indicate a tilt of the whole molecule in a disordered multilayer, the monolayer will be used to analyze the adsorption geometry of the Cu-TPP on the surface." the monolayer will be used to analyze the adsorption geometry of the Cu-TPP

on the surface. Compared with the multilayer both the nitrogen (Fig. 4d) and the carbon region (Fig. 5d) of the monolayer show a broadening of the peaks, though the changes are not quite as big as for the 2H-TPP which indicates a weaker interaction of the Cu-TPP with the copper substrate. In the N-edge spectra the first resonance (peak A') is not quenched which leads to the conclusion that no electron transfer to the LUMO occurs in this case. The fit of the N-edge region is easier as in the case of 2H-TPP but still not as convenient as for the multilayer. It gives a tilting angle of 10°-20° for the pyrrole rings which means that the macrocycle of the adsorbed Cu-TPP is considerably less distorted than that of the free-base porphyrin. The analysis of the carbon region again proves to be more difficult because of the peak broadening and the large number of contributing resonances: the fit is divided in a macrocycle and a phenyl part which results in angles of α_{ph} = 40°-50° for the phenyl rings and α_{mac} = 10°-20° for the macrocycle supporting the fit of the N-edge region. Table III compares the results of the mono- and multilayer fits with the respective values of the 2H-TPP samples. The metalation thus leads to a conformational change from a free-base porphyrin with a strongly deformed macrocycle and rather flat phenyl rings to a Cu-TPP with a nearly planar macrocycle and stronger tilted phenyl rings (Fig. 10b).

V. CONCLUSIONS

Our results demonstrate that a combination of theoretical and experimental spectroscopy methods allows a detailed analysis of the differences between mono- and multilayer films of metalated and non-metalated tetraphenylporphyrins. We showed that for 2H-TPP on Cu(111) self-metalation, i.e., the direct metalation of free-base porphyrin molecules with substrate atoms, is possible. Annealing of 2H-TPP mono- and multilayer films to a temperature of 420 K leads to changes in XPS and NEXAFS signatures which are mainly related

to the macrocycle. By comparing the experimental data to XPS results and NEXAFS spectra obtained by transition potential DFT calculations these changes are attributed to the coordination of the nitrogen atoms with copper from the substrate. The comparison of the experimental NEXAFS curves with the simulated spectra shows that the main transitions and final state orbitals are very similar for 2H-TPP and Cu-TPP, suggesting that the dissimilarity of the respective monolayer spectra originate from differences in the interaction of free-base and metalloporphyrins with the substrate. Angle resolved measurements reveal the strong influence of the copper surface on the 2H-TPP molecules resulting in a conformation with a strongly distorted macrocycle and nearly flat phenyl rings. The quenching of the lowest NEXAFS resonance in the monolayer suggests an electron transfer to the LUMO. In contrast, for Cu-TPP the experimental data show no such charge transfer and NEXAFS measurements point to a relaxed macrocycle of the metalloporphyrin indicating a modified molecule-substrate interaction.

VI. ACKNOWLEDGMENTS

This work was supported by the European Research Council (ERC Advanced Grant MolArt). We acknowledge the Helmholtz-Zentrum Berlin-Electron storage ring BESSY II for provision of synchrotron radiation at beamline HE-SGM. Traveling cost for the BESSY measurements provided by Helmholtz-Zentrum Berlin are gratefully acknowledged.

REFERENCES

[a]corresponding author: katharina.diller@tum.de

[1]H. Ishii, K. Sugiyama, E. Ito, and K. Seki, Adv. Mater. **11**, 605 (1999).

[2]J. V. Barth, Annu. Rev. Phys. Chem. **58**, 375 (2007).

[3]T. A. Jung, R. R. Schlittler, and J. K. Gimzewski, Nature **386**, 696 (1997).

[4]H. Wende, M. Bernien, J. Luo, C. Sorg, N. Ponpandian, J. Kurde, J. Miguel, M. Piantek, X. Xu, P. Eckhold, W. Kuch, K. Baberschke, P. M. Panchmatia, B. Sanyal, P. M. Oppeneer, and O. Eriksson, Nat. Mater. **6**, 516 (2007).

[5]A. Hauschild, K. Karki, B. C. C. Cowie, M. Rohlfing, F. S. Tautz, and M. Sokolowski, Phys. Rev. Lett. **94**, 036106 (2005).

[6]L. Romaner, G. Heimel, J.-L. Brédas, A. Gerlach, F. Schreiber, R. L. Johnson, J. Zegenhagen, S. Duhm, N. Koch, and E. Zojer, Phys. Rev. Lett. **99**, 256801 (2007).

[7]J. A. A. W. Elemans, R. van Hameren, R. J. M. Nolte, and A. E. Rowan, Adv. Mater **18**, 1251 (2006).

[8]S. Koiry, P. Jha, D. Aswal, S. Nayak, C. Majumdar, S. Chattopadhyay, S. Gupta, and J. Yakhmi, Chem. Phys. Lett. **485**, 137 (2010).

[9]N. A. Rakow and K. S. Suslick, Nature **406**, 710 (2000).

[10]D. Filippini, A. Alimelli, C. Di Natale, R. Paolesse, A. D'Amico, and I. Lundström, Angew. Chem. Int. Ed. **45**, 3800 (2006).

[11]B. Meunier, Chem. Rev. **92**, 1411 (1992).

[12]I. Mochida, K. Suetsugu, H. Fujitsu, and K. Takeshita, J. Phys. Chem. **87**, 1524 (1983).

[13]I. Bhugun, D. Lexa, and J.-M. Savéant, J. Am. Chem. Soc. **118**, 3982 (1996).

[14]W. M. Campbell, A. K. Burrell, D. L. Officer, and K. W. Jolley, Coord. Chem. Rev. **248**, 1363 (2004).

[15]P. Vilmercati, C. C. Cudia, R. Larciprete, C. Cepek, G. Zampieri, L. Sangaletti, S. Pagliara, A. Verdini, A. Cossaro, L. Floreano, A. Morgante, L. Petaccia, S. Lizzit, C. Battocchio, G. Polzonetti, and A. Goldoni, Surf. Sci. **600**, 4018 (2006).

[16]M. A. Baldo, D. F. O'Brien, Y. You, A. Shoustikov, S. Sibley, M. E. Thompson, and S. R. Forrest, Nature **395**, 151 (1998).

[17]K. Flechtner, A. Kretschmann, H.-P. Steinrück, and J. M. Gottfried, J. Am. Chem. Soc. **129**, 12110 (2007).

[18]J. V. Barth, Surf. Sci. **603**, 1533 (2009).

[19]M. Gottfried and H. Marbach, Z. Phys. Chem. **223**, 53 (2009).

[20]W. Hieringer, K. Flechtner, A. Kretschmann, K. Seufert, W. Auwärter, J. V. Barth, A. Görling, H.-P. Steinrück, and J. M. Gottfried, J. Am. Chem. Soc. **133**, 6206 (2011).

[21]S. Haq, F. Hanke, M. S. Dyer, M. Persson, P. Iavicoli, D. B. Amabilino, and R. Raval, J. Am. Chem. Soc. **133**, 12031 (2011).

[22]T. Lukasczyk, K. Flechtner, L. R. Merte, N. Jux, F. Maier, J. M. Gottfried, and H.-P. Steinrück, J. Phys. Chem. C **111**, 3090 (2007).

[23]K. Leung, S. B. Rempe, P. A. Schultz, E. M. Sproviero, V. S. Batista, M. E. Chandross, and C. J. Medforth, J. Am. Chem. Soc. **128**, 3659 (2006).

[24]S. Müllegger, W. Schöfberger, M. Rashidi, T. Lengauer, F. Klappenberger, K. Diller, K. Kara, J. V. Barth, E. Rauls, W. G. Schmidt, and R. Koch, ACS Nano **5**, 6480 (2011).

[25]T. Yokoyama, T. Kamikado, S. Yokoyama, and S. Mashiko, J. Chem. Phys. **121**, 11993 (2004).

[26]D. Heim, K. Seufert, W. Auwärter, C. Aurisicchio, C. Fabbro, D. Bonifazi, and J. V. Barth, Nano Lett. **10**, 122 (2010).

[27]K. Seufert, W. Auwärter, and J. V. Barth, J. Am. Chem. Soc. **132**, 18141 (2010).

[28]K. Seufert, M.-L. Bocquet, W. Auwärter, A. Weber-Bargioni, J. Reichert, N. Lorente, and J. V. Barth, Nat Chem **3**, 114 (2011).

[29]W. Auwärter, K. Seufert, F. Klappenberger, J. Reichert, A. Weber-Bargioni, A. Verdini, D. Cvetko, M. Dell'Angela, L. Floreano, A. Cossaro, G. Bavdek, A. Morgante, A. P. Seitsonen, and J. V. Barth, Phys. Rev. B **81**, 245403 (2010).

[30]W. Auwärter, A. Weber-Bargioni, S. Brink, A. Riemann, A. Schiffrin, M. Ruben, and J. V. Barth, ChemPhysChem **8**, 250 (2007).

[31]D. Écija, M. Trelka, C. Urban, P. d. Mendoza, E. Mateo-Martí, C. Rogero, J. A. Martín-Gago, A. M. Echavarren, R. Otero, J. M. Gallego, and R. Miranda, J. Phys. Chem. C **112**, 8988 (2008).

[32]G. Di Santo, C. Castellarin-Cudia, M. Fanetti, B. Taleatu, P. Borghetti, L. Sangaletti, L. Floreano, E. Magnano, F. Bondino, and A. Goldoni, J. Phys. Chem. C **115**, 4155 (2011).

[33]T. E. Shubina, H. Marbach, K. Flechtner, A. Kretschmann, N. Jux, F. Buchner, H. Steinrück, T. Clark, and J. M. Gottfried, J. Am. Chem. Soc. **129**, 9476–9483 (2007).

[34]J. M. Gottfried, K. Flechtner, A. Kretschmann, T. Lukasczyk, and H.-P. Steinrück, J. Am. Chem. Soc. **128**, 5644 (2006).

[35]M. Chen, X. Feng, L. Zhang, H. Ju, Q. Xu, J. Zhu, J. M. Gottfried, K. Ibrahim, H. Qian, and J. Wang, J. Phys. Chem. C **114**, 9908 (2010).

[36]A. Weber-Bargioni, J. Reichert, A. P. Seitsonen, W. Auwärter, A. Schiffrin, and J. V. Barth, J. Phys. Chem. C **112**, 3453 (2008).

[37]D. Écija, W. Auwärter, S. Vijayaraghavan, K. Seufert, F. Bischoff, K. Tashiro, and J. V. Barth, Angew. Chem. Int. Ed. **50**, 3872 (2011).

[38]R. González-Moreno, C. Sánchez-Sánchez, M. Trelka, R. Otero, A. Cossaro, A. Verdini, L. Floreano, M. Ruiz-Bermejo, A. García-Lekue, J. Martín-Gago, and C. Rogero, J. Phys. Chem. C **115**, 6849–6854 (2011).

[39]C. C. Cudia, P. Vilmercati, R. Larciprete, C. Cepek, G. Zampieri, L. Sangaletti, S. Pagliara, A. Verdini, A. Cossaro, L. Floreano, A. Morgante, L. Petaccia, S. Lizzit, C. Battocchio, G. Polzonetti, and A. Goldoni, Surf. Sci. **600**, 4013 (2006).

[40]F. Klappenberger, A. Weber-Bargioni, W. Auwärter, M. Marschall, A. Schiffrin, and J. V. Barth, J. Chem. Phys. **129**, 214702 (2008).

[41]S. Krasnikov, A. Preobrajenski, N. Sergeeva, M. Brzhezinskaya, M. Nesterov, A. Cafolla, M. Senge, and A. Vinogradov, Chem. Phys. **332**, 318 (2007).

[42]A. Weber-Bargioni, W. Auwärter, F. Klappenberger, J. Reichert, S. Lefrancois, T. Strunskus, C. Wöll, A. Schiffrin, Y. Pennec, and J. V. Barth, ChemPhysChem **9**, 89 (2008).

[43]S. Narioka, H. Ishii, Y. Ouchi, T. Yokoyama, T. Ohta, and K. Seki, J. Phys. Chem. **99**, 1332 (1995).

[44]G. Polzonetti, V. Carravetta, G. Iucci, A. Ferri, G. Paolucci, A. Goldoni, P. Parent, C. Laffon, and M. V. Russo, Chem. Phys. **296**, 87 (2004).

[45]N. Schmidt, R. Fink, and W. Hieringer, J. Chem. Phys. **133**, 054703 (2010).

[46]J. Stöhr, *NEXAFS Spectroscopy*, edited by R. Gomer (Springer, 1992).

[47]"StoBe is a modified version of the DFT-LCGTO program package DeMon, originally developed by A. St.-Amant and D. Salahub (University of Montreal), with extensions by K. Hermann and L.G.M. Pettersson.".

[48]B. Hammer, L. B. Hansen, and J. K. Nørskov, Phys. Rev. B **59**, 7413 (1999).

[49]J. P. Perdew, K. Burke, and M. Ernzerhof, Phys. Rev. Lett. **77**, 3865 (1996).

[50]T. H. Dunning, J. Chem. Phys. **55**, 716 (1971).

[51]S. Huzinaga, J. Chem. Phys. **42**, 1293 (1965).

[52]W. Auwärter, F. Klappenberger, A. Weber-Bargioni, A. Schiffrin, T. Strunskus, C. Wöll, Y. Pennec, A. Riemann, and J. V. Barth, J. Am. Chem. Soc. **129**, 11279 (2007).

[53]E. B. Fleischer, J. Am. Chem. Soc. **85**, 1353–1354 (1963).

[54]E. B. Fleischer, Accounts Chem. Res. **3**, 105–112 (1970).

[55]W. Kutzelnigg, U. Fleischer, and M. Schindler, in: NMR Basic Principles and Progress, Springer Verlag, Berlin/Heidelberg **213**, 165 (1991).

[56]L. G. M. Pettersson, U. Wahlgren, and O. Gropen, J. Chem. Phys. **86**, 2176 (1987).

[57]L. G. M. Pettersson, U. Wahlgren, and O. Gropen, Chem. Phys. **80**, 7 (1983).

[58]H. Ågren, V. Carravetta, O. Vahtras, and L. G. M. Pettersson, Theoretica Chimica Acta **97**, 14 (1997).

[59]J. C. Slater, Adv. Quant. Chem. **6**, 1 (1972).

[60]L. Triguero, L. G. M. Pettersson, and H. Ågren, Phys. Rev. B **58**, 8097 (1998).

[61]O. Takahashi and L. G. M. Pettersson, J. Chem. Phys. **121**, 10339 (2004).

[62]Y. Niwa, H. Kobayashi, and T. Tsuchiya, J. Chem. Phys. **60**, 799 (1974).

[63]J. P. Macquet, M. M. Millard, and T. Theophanides, J. Am. Chem. Soc. **100**, 4741 (1978).

[64]T.-C. Chiang, G. Kaindl, and T. Mandel, Phys. Rev. B **33**, 695 (1986).

[65]D. H. Karweik and N. Winograd, Inorg. Chem. **15**, 2336 (1976).

[66]R. Dippel, D. P. Woodruff, X. M. Hu, M. C. Asensio, A. W. Robinson, K. M. Schindler, K. U. Weiss, P. Gardner, and A. M. Bradshaw, Phys. Rev. Lett. **68**, 1543 (1992).

[67]K. U. Weiss, R. Dippel, K. M. Schindler, P. Gardner, V. Fritzsche, A. M. Bradshaw, A. L. D. Kilcoyne, and D. P. Woodruff, Phys. Rev. Lett. **69**, 3196 (1992).

[68]C. J. Hirschmugl, K. M. Schindler, O. Schaff, V. Fernandez, A. Theobald, P. Hofmann, A. M. Bradshaw, R. Davis, N. A. Booth, D. P. Woodruff, and V. Fritzsche, Surf. Sci. **352**, 232 (1996).

[69]M. Eichberger, M. Marschall, J. Reichert, A. Weber-Bargioni, W. Auwärter, R. L. C. Wang, H. J. Kreuzer, Y. Pennec, A. Schiffrin, and J. V. Barth, Nano Lett. **8**, 4608 (2008).

[70]L. Scudiero, D. E. Barlow, and K. W. Hipps, J. Phys. Chem. B **104**, 11899 (2000).

[71]A. D. Zhao, Q. X. Li, L. Chen, H. J. Xiang, W. H. Wang, S. Pan, B. Wang, X. D. Xiao, J. L. Yang, J. G. Hou, and Q. S. Zhu, Science **309**, 1542 (2005).

[72]M. Ruben, D. Payer, A. Landa, A. Comisso, C. Gattinoni, N. Lin, J. P. Collin, J. P. Sauvage, A. De Vita, and K. Kern, J. Am. Chem. Soc. **128**, 15644 (2006).

[73]A. Sperl, J. Kröger, and R. Berndt, Angew. Chem. Int. Ed. **123**, 5406 (2011).

[74]M. E. Cañas-Ventura, F. Klappenberger, S. Clair, S. Pons, K. Kern, H. Brune, T. Strunskus, C. Wöll, R. Fasel, and J. V. Barth, J. Chem. Phys. **125**, 184710 (2006).

[75]I. Reid, Y. Zhang, A. Demasi, A. Blueser, L. Piper, J. E. Downes, A. Matsuura, G. Hughes, and K. E. Smith, Appl. Surf. Sci. **256**, 720 (2009).

[76]H. Häkkinen and M. Manninen, Phys. Rev. B **46**, 1725 (1992).

[77]G. C. Kallinteris, G. A. Evangelakis, and N. I. Papanicolaou, Surf. Sci. **369**, 185 (1996).

[78]M. Giesen, Surf. Sci. **442**, 543 (1999).

[79]M. Giesen and G. Schulze Icking-Konert, Surf. Sci. **412-413**, 645 (1998).

[80]J. Kołaczkiewicz, Surf. Sci. **183**, 251 (1987).

[81]H. Walch, J. Dienstmaier, G. Eder, R. Gutzler, S. Schlögl, T. Sirtl, K. Das, M. Schmittel, and M. Lackinger, J. Am. Chem. Soc. **133**, 7909 (2011).

[82]C. M. Doyle, S. A. Krasnikov, N. N. Sergeeva, A. B. Preobrajenski, N. A. Vinogradov, Y. N. Sergeeva, M. O. Senge, and A. A. Cafolla, Chem. Commun. **47**, 12134 (2011).

[83]F. Buchner, K. Flechtner, Y. Bai, E. Zillner, I. Kellner, H.-P. Steinrück, H. Marbach, and J. M. Gottfried, J. Phys. Chem. C **112**, 15458 (2008).

[84]A. Gölzhäuser, S. Panov, M. Mast, A. Schertel, M. Grunze, and C. Wöll, Surf. Sci. **334**, 235 (1995).

[85]G. Rojas, X. Chen, C. Bravo, J.-H. Kim, J.-S. Kim, J. Xiao, P. A. Dowben, Y. Gao, X. C. Zeng, W. Choe, and A. Enders, J. Phys. Chem. C **114**, 9408 (2010).

[86]F. Buchner, E. Zillner, M. Röckert, S. Gläßel, H.-P. Steinrück, and H. Marbach, Chem. Eur. J. **17**, 10226 (2011).

[87]D. Duflot, J. P. Flament, J. Heinesch, and M. J. Hubin-Franskin, J. Electron Spectrosc. Relat. Phenom. **113**, 79 (2000).

[88]S. A. Krasnikov, N. N. Sergeeva, M. M. Brzhezinskaya, A. B. Preobrajenski, Y. N. Sergeeva, N. A. Vinogradov, A. A. Cafolla, M. O. Senge, and A. S. Vinogradov, J. Phys.: Condens. Matter **20**, 235207 (2008).

[89]T.-C. Tseng, C. Urban, Y. Wang, R. Otero, S. L. Tait, M. Alcamí, D. Écija, M. Trelka, J. M. Gallego, N. Lin, M. Konuma, U. Starke, A. Nefedov, A. Langner, C. Wöll, M. Ángeles Herranz, F. Martín, N. Martín, K. Kern, and R. Miranda, Nat. Chem. **2**, 374–379 (2010).

[90]A. P. Hitchcock, J. A. Horsley, and J. Stöhr, J. Chem. Phys. **85**, 4835 (1986).

[91]J. Brede, M. Linares, R. Lensen, A. E. Rowan, M. Funk, M. Broring, G. Hoffmann, and R. Wiesendanger, J. Vac. Sci. Technol. B **27**, 799 (2009).

[92]A. Rosa, G. Ricciardi, and E. J. Baerends, J. Phys. Chem. A **110**, 5180 (2006).

[93]T. Yokoyama, S. Yokoyama, T. Kamikado, and S. Mashiko, J. Chem. Phys. **115**, 3814 (2001).

[94]W. Auwärter, A. Weber-Bargioni, A. Riemann, A. Schiffrin, O. Gröning, R. Fasel, and J. V. Barth, J. Chem. Phys. **124**, 194708 (2006).

[95]S. A. Krasnikov, N. N. Sergeeva, Y. N. Sergeeva, M. O. Senge, and A. A. Cafolla, Phys. Chem. Chem. Phys. **12**, 6666 (2010).

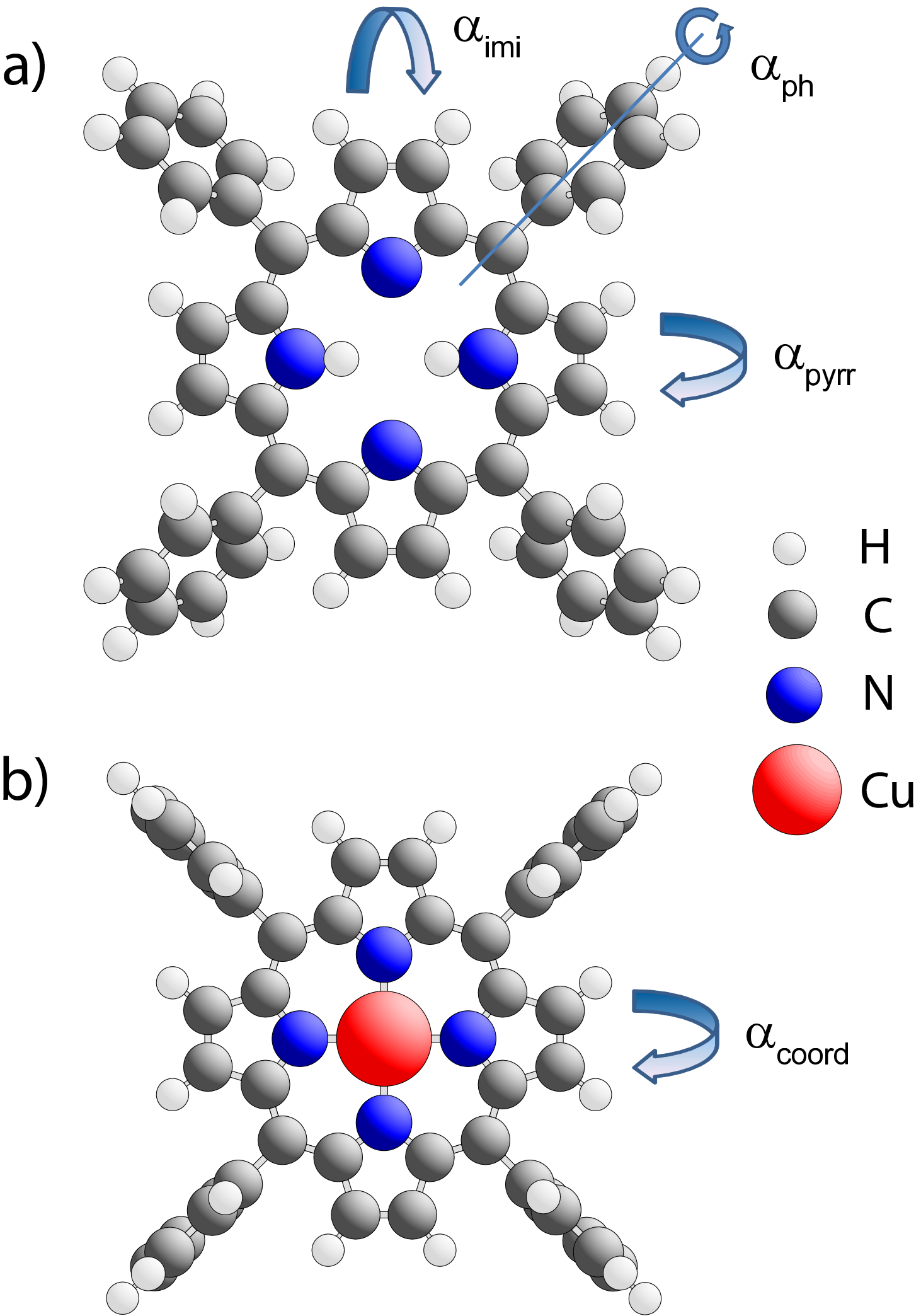
a)
α_{imi}
α_{ph}
α_{pyrr}
H
C
N
b)
Cu
α_{coord}

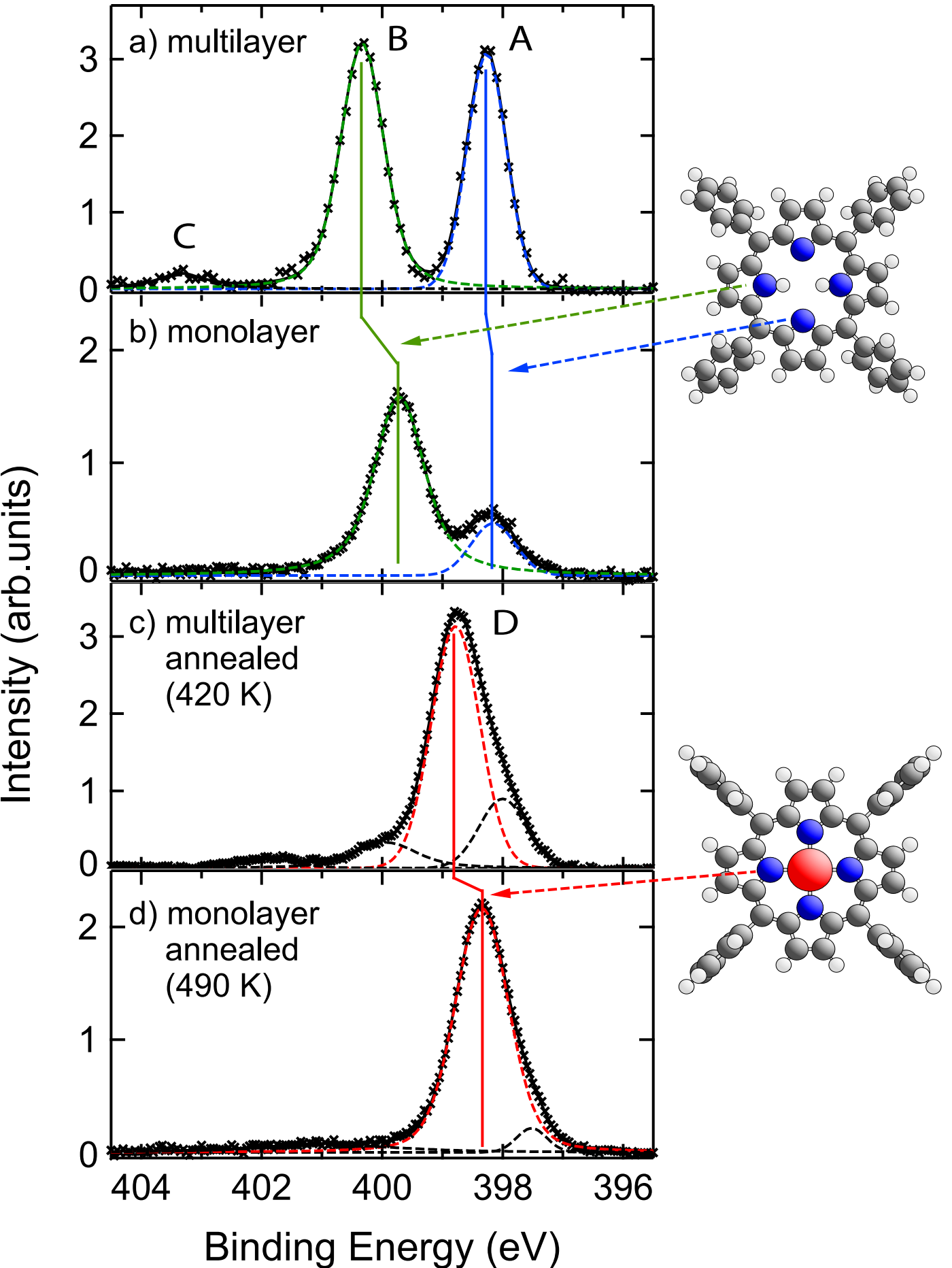
a) multilayer
B
A
C
b) monolayer
c) multilayer
annealed
(420 K)
D
d) monolayer
annealed
(490 K)
Intensity (arb.units)
Binding Energy (eV)
404
402
400
398
396

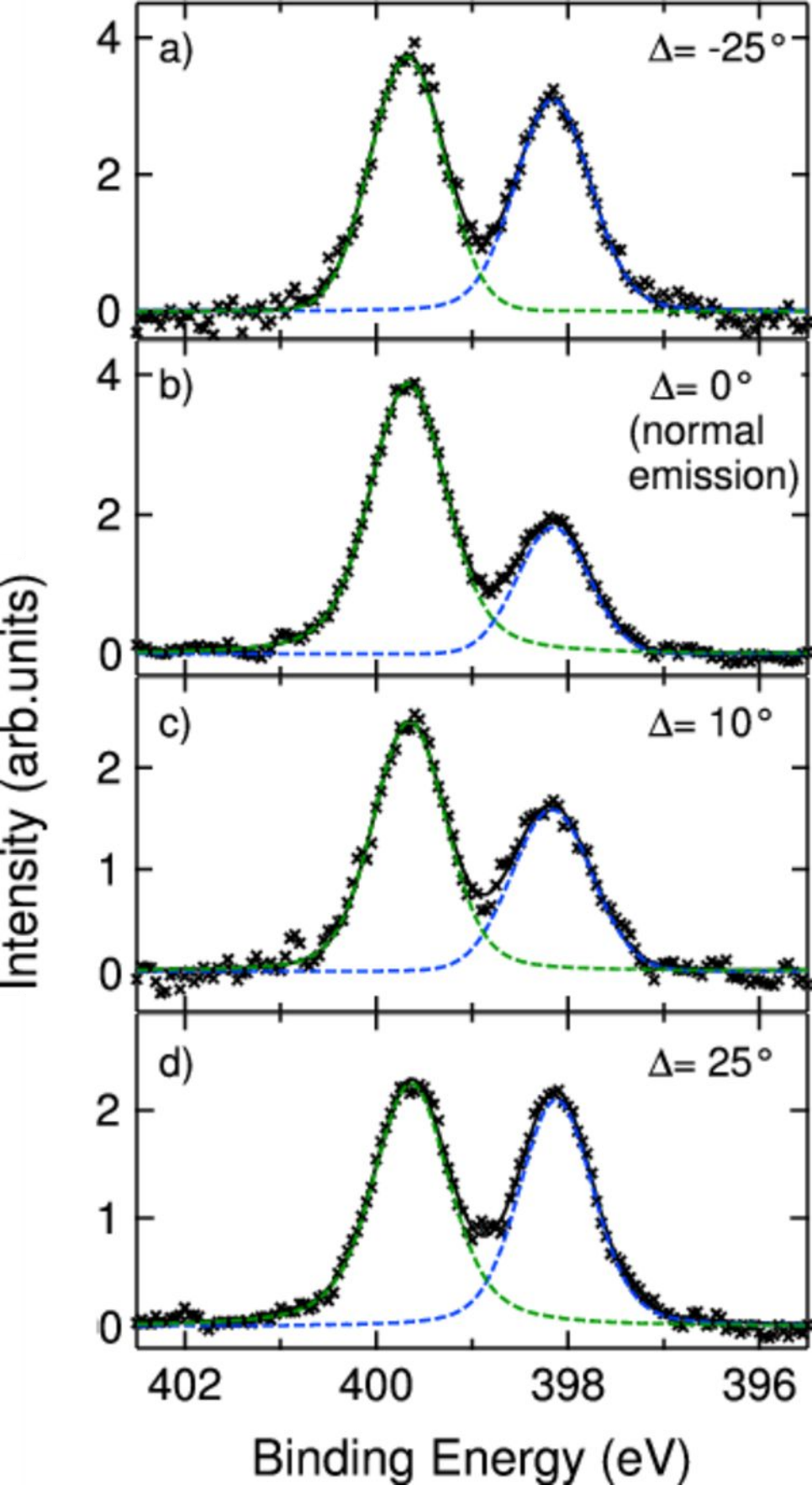
a)
Δ= -25°
b)
Δ= 0°
(normal
emission)
c)
Δ= 10°
d)
Δ= 25°
Intensity (arb.units)
Binding Energy (eV)
402
400
398
396

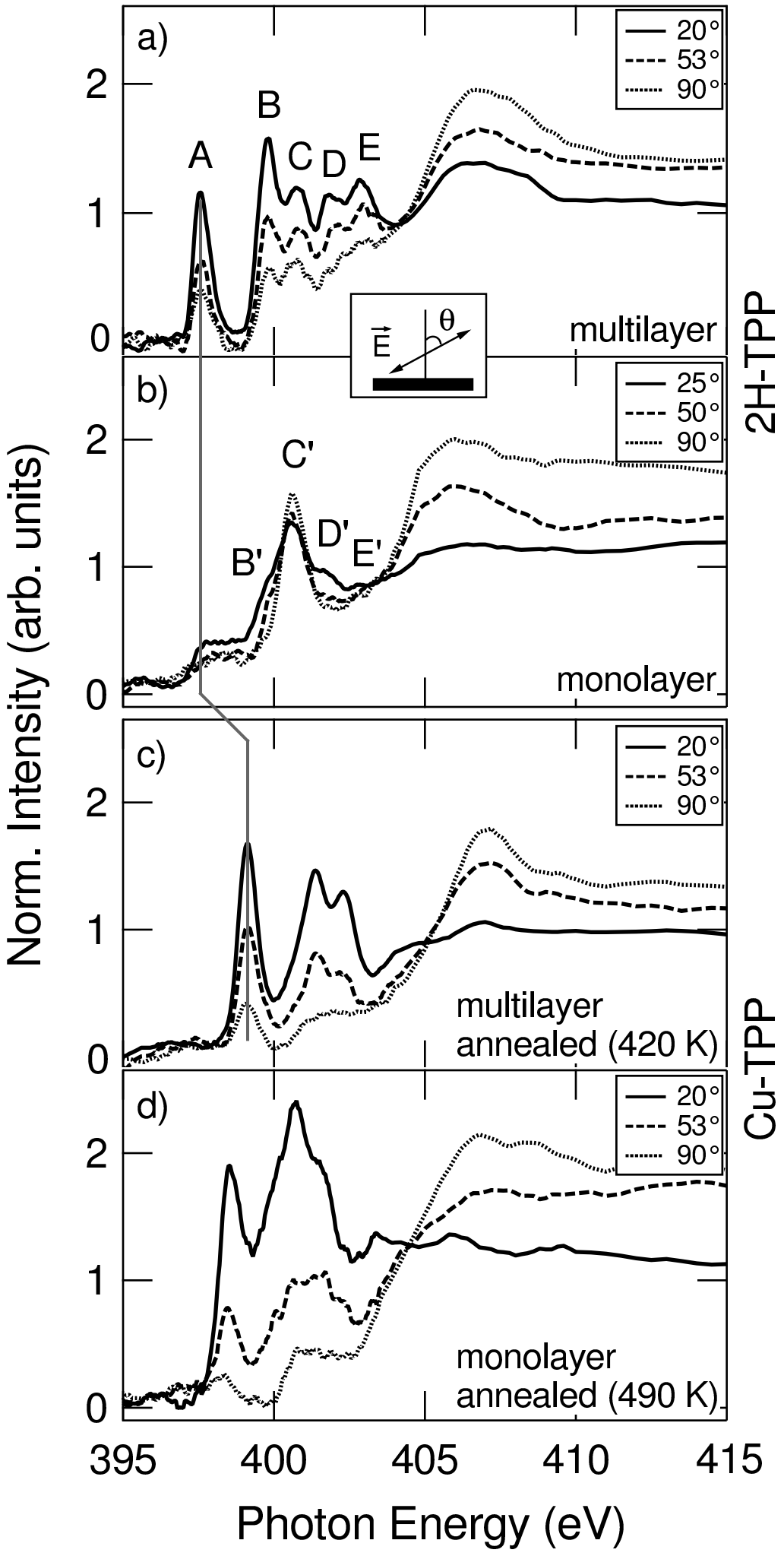
a)
20°
53°
90°
A
B
C
D
E
θ
E
multilayer
b)
25°
50°
90°
C'
B'
D'
E'
monolayer
2H-TPP
c)
20°
53°
90°
multilayer
annealed (420 K)
d)
20°
53°
90°
monolayer
annealed (490 K)
Cu-TPP
Norm. Intensity (arb. units)
0
1
2
395
400
405
410
415
Photon Energy (eV)

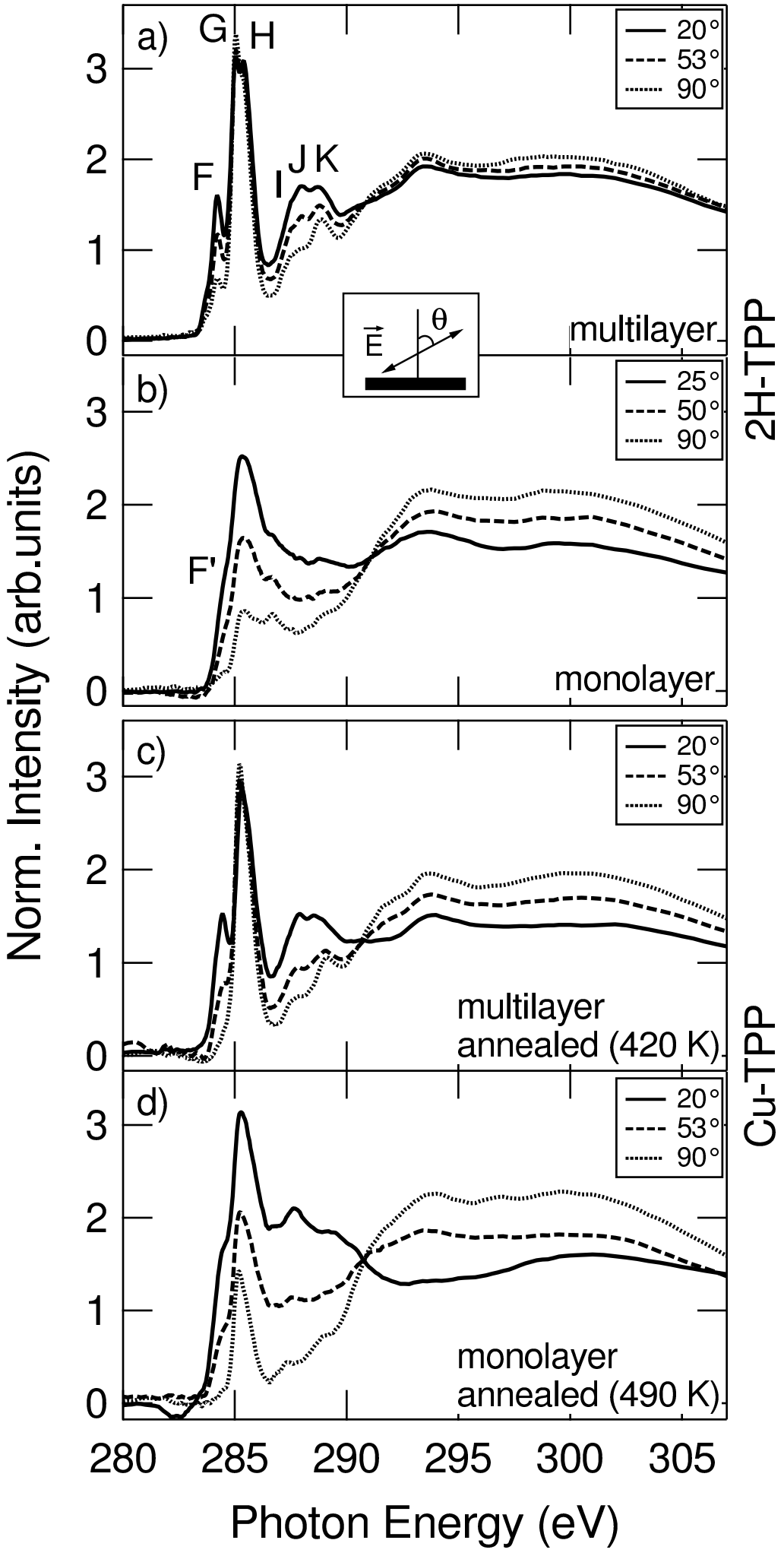
a)
G
H
F
I
J
K
20°
53°
90°
multilayer
θ
E
b)
25°
50°
90°
F'
monolayer
2H-TPP
c)
20°
53°
90°
multilayer
annealed (420 K)
d)
20°
53°
90°
monolayer
annealed (490 K)
Cu-TPP
Norm. Intensity (arb.units)
0
1
2
3
280
285
290
295
300
305
Photon Energy (eV)

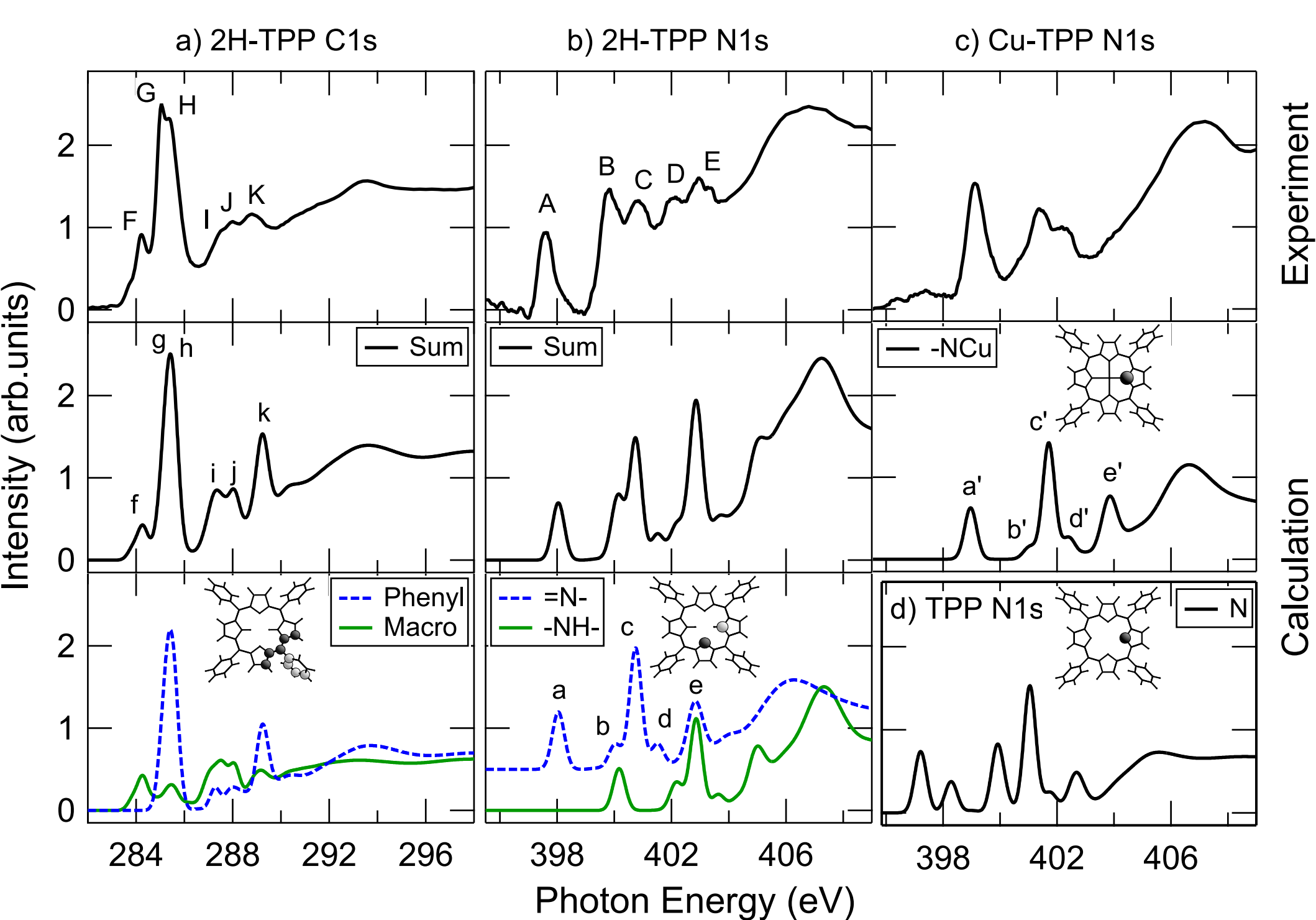
a) 2H-TPP C1s
b) 2H-TPP N1s
c) Cu-TPP N1s
Experiment
Calculation
Intensity (arb.units)
Photon Energy (eV)
G
H
F
I
J
K
A
B
C
D
E
g
h
f
i
j
k
Sum
-NCu
c'
a'
b'
d'
e'
Phenyl
Macro
=N-
-NH-
a
b
c
d
e
d) TPP N1s
N
0
1
2
284
288
292
296
398
402
406

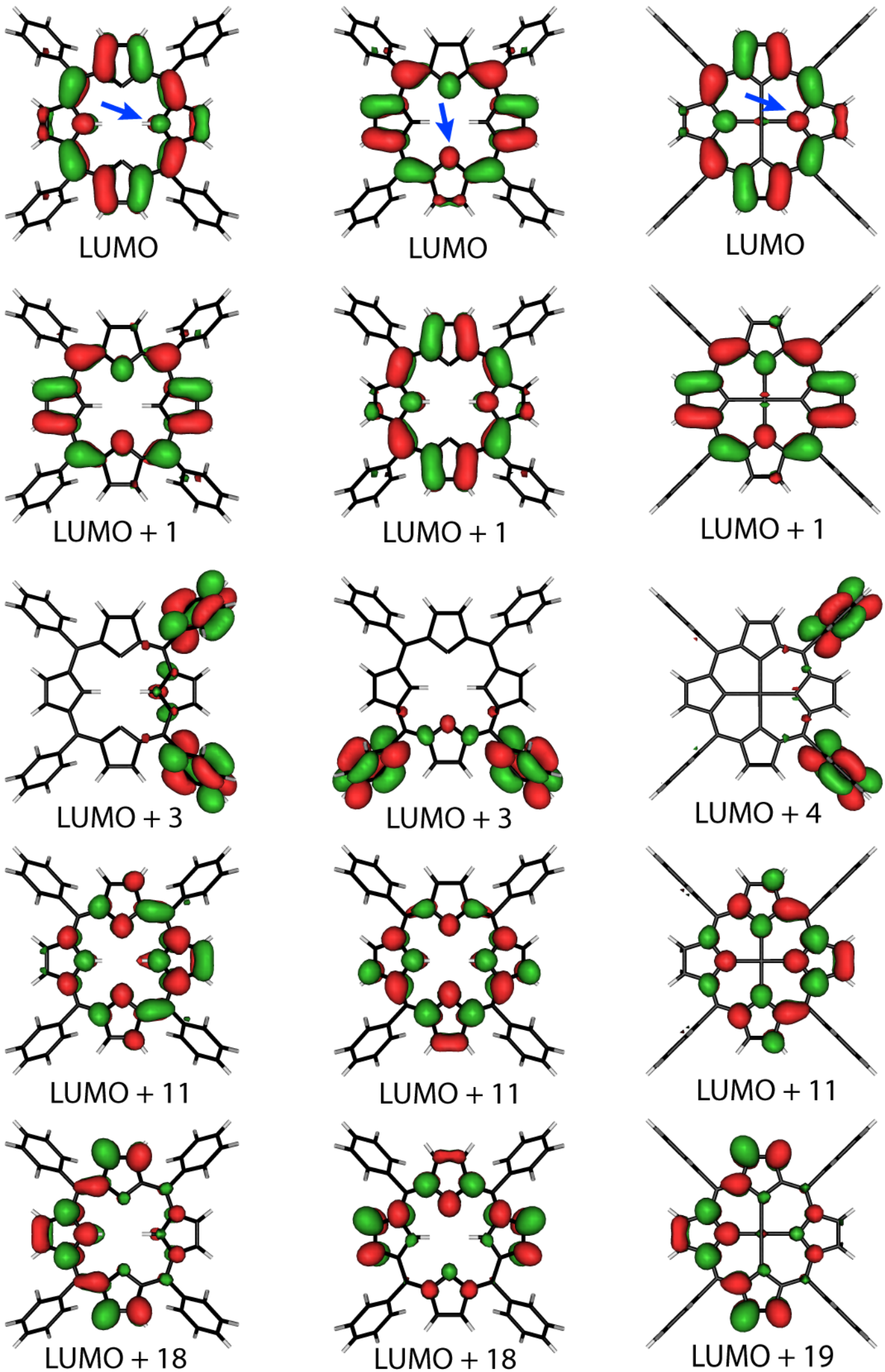
a) 2H-TPP (-NH-)
b) 2H-TPP (=N-)
c) Cu-TPP (N-Cu)
LUMO
LUMO
LUMO
LUMO + 1
LUMO + 1
LUMO + 1
LUMO + 3
LUMO + 3
LUMO + 4
LUMO + 11
LUMO + 11
LUMO + 11
LUMO + 18
LUMO + 18
LUMO + 19

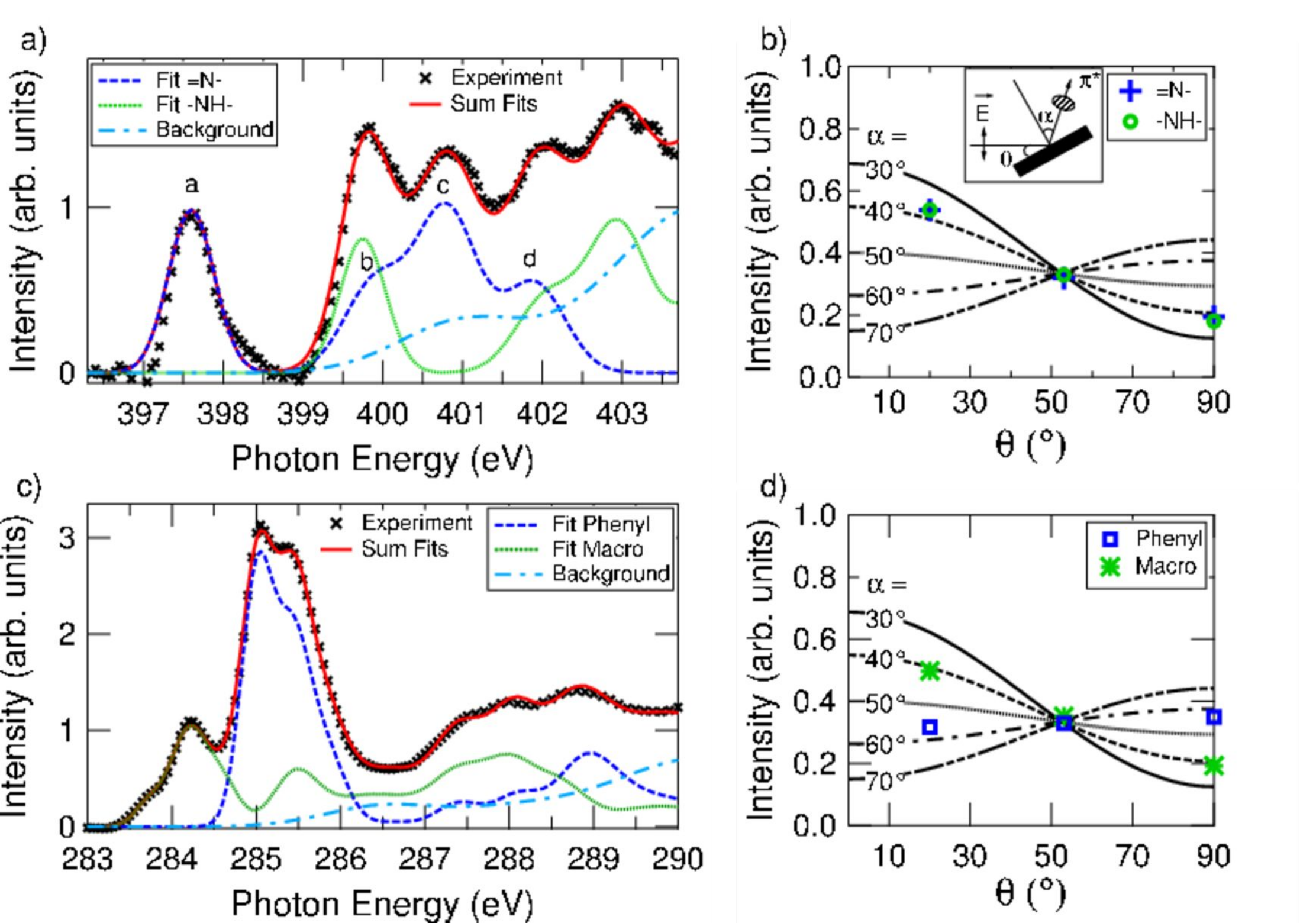
a)
Fit =N-
Fit -NH-
Background
Experiment
Sum Fits
a
b
c
d
Intensity (arb. units)
Photon Energy (eV)
b)
=N-
-NH-
α =
30°
40°
50°
60°
70°
E
α
π*
θ
Intensity (arb. units)
θ (°)
c)
Experiment
Sum Fits
Fit Phenyl
Fit Macro
Background
Intensity (arb. units)
Photon Energy (eV)
d)
Phenyl
Macro
α =
30°
40°
50°
60°
70°
Intensity (arb. units)
θ (°)

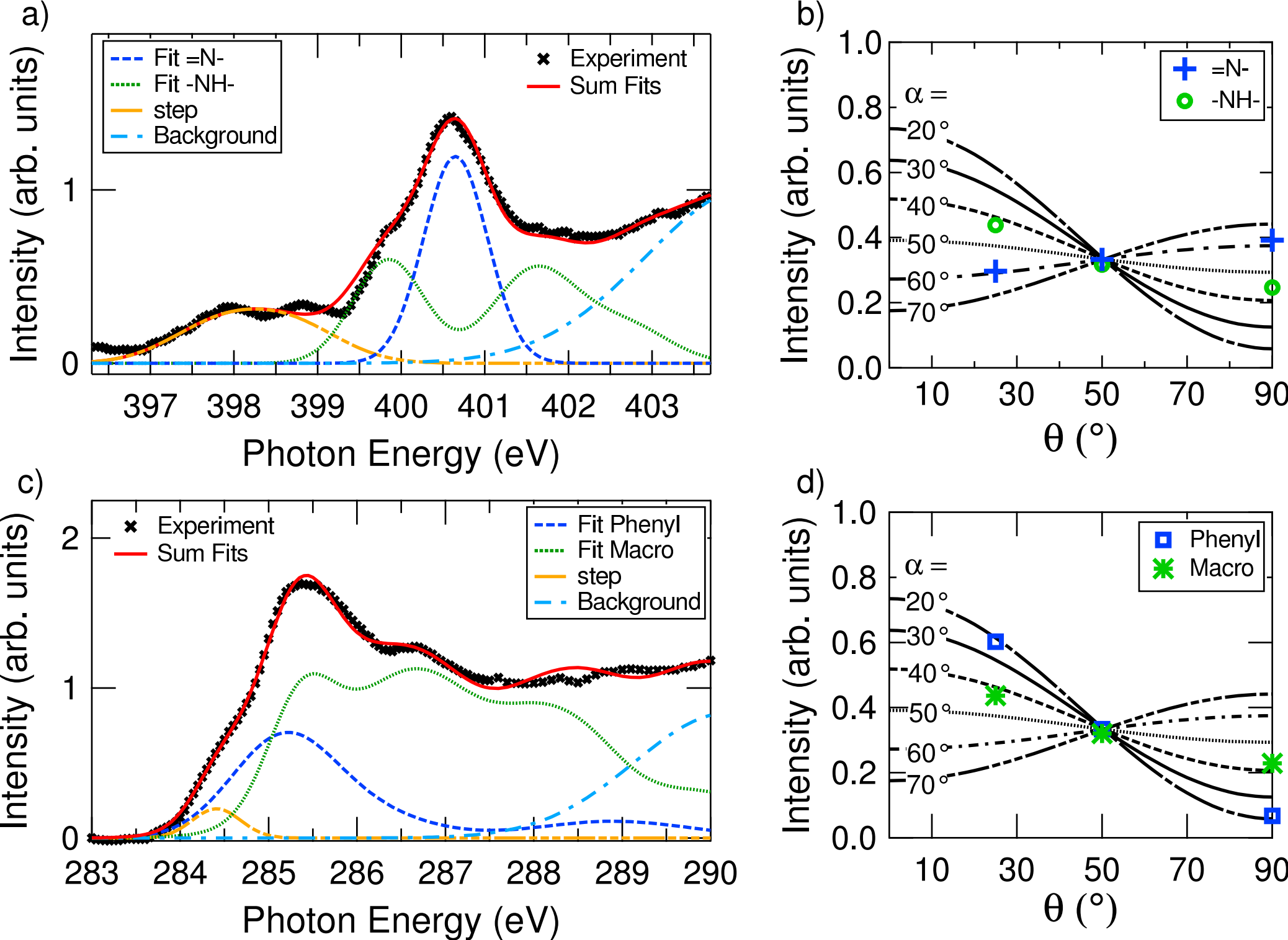
a)
Fit =N-
Fit -NH-
step
Background
Experiment
Sum Fits
Intensity (arb. units)
Photon Energy (eV)
b)
=N-
-NH-
α =
20°
30°
40°
50°
60°
70°
Intensity (arb. units)
θ (°)
c)
Experiment
Sum Fits
Fit Phenyl
Fit Macro
step
Background
Intensity (arb. units)
Photon Energy (eV)
d)
Phenyl
Macro
α =
20°
30°
40°
50°
60°
70°
Intensity (arb. units)
θ (°)

a) 2H-TPP

b) Cu-TPP